AD-A074 440 VIRGINIA UNIV CHARLOTTESVILLE DEPT OF MATERIALS SCIENCE F/G 11/6
INVESTIGATION OF ELONGATION AND ITS RELATIONSHIP TO RESIDUAL ST--ETC(U)
SEP 79 F E WAWNER, J W EASON, R A JOHNSON N00014-76-C-0694
UNCLASSIFIED UVA/525322/MS79/102 NL

1 OF 2
AD A074440

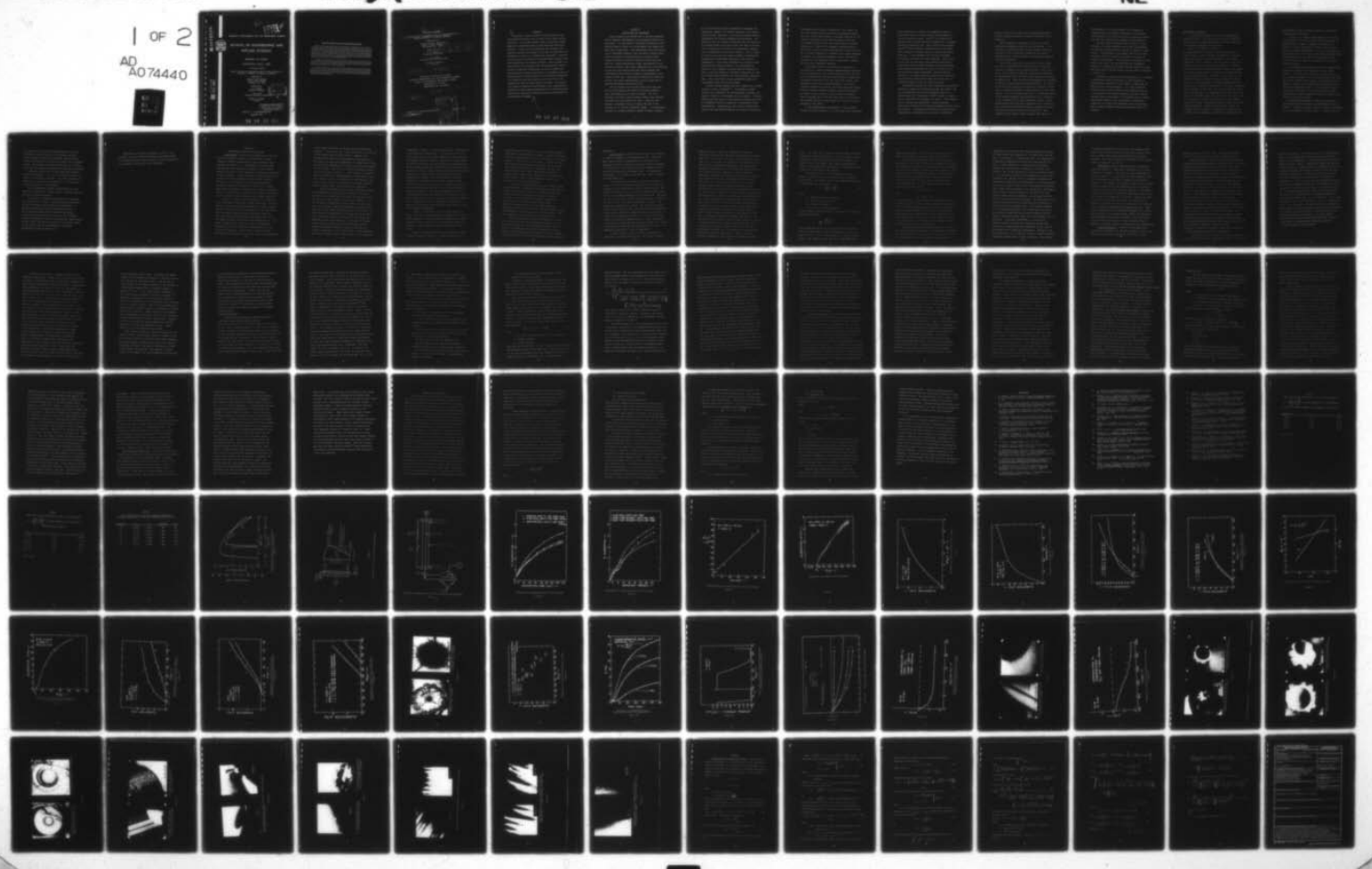

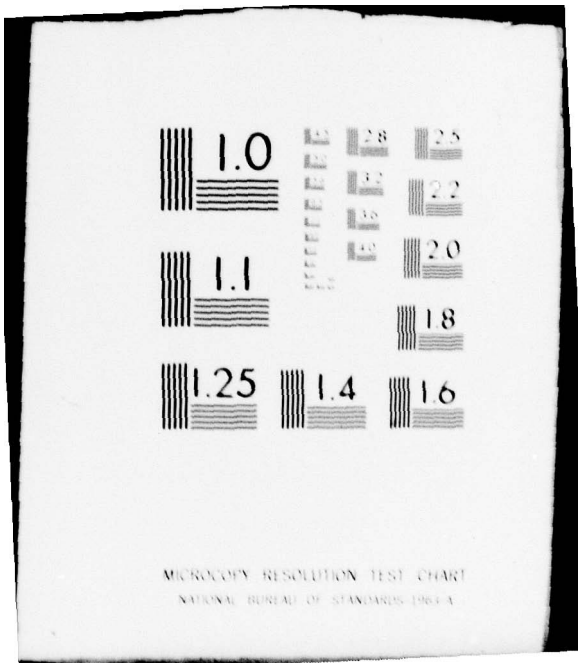
1.0
1.1
1.25
1.4
1.6
2.0
1.8
MICROCOPY RESOLUTION TEST CHART
NATIONAL BUREAU OF STANDARDS 1963-A

AD A074440

DDC FILE COPY

(12)
A056528
LEVEL

RESEARCH LABORATORIES FOR THE ENGINEERING SCIENCES

SCHOOL OF ENGINEERING AND APPLIED SCIENCE

UNIVERSITY OF VIRGINIA

Charlottesville, Virginia 22901

A Technical Report

INVESTIGATION OF ELONGATION AND ITS RELATIONSHIP TO RESIDUAL STRESSES IN BORON FILAMENTS

Submitted to:

Office of Naval Research
800 N. Quincy Street
Arlington, VA 22217

DDC
RECEIVED
SEP 28 1979
A

Submitted by:

F. E. Wawner
Research Professor

J. W. Eason
Graduate Research Assistant

Robert A. Johnson
Professor

DISTRIBUTION STATEMENT A
Approved for public release
Distribution Unlimited

Report No. UVA/525322/MS79/102

September 1979

79 09 27 011

RESEARCH LABORATORIES FOR THE ENGINEERING SCIENCES

Members of the faculty who teach at the undergraduate and graduate levels and a number of professional engineers and scientists whose primary activity is research generate and conduct the investigations that make up the school's research program. The School of Engineering and Applied Science of the University of Virginia believes that research goes hand in hand with teaching. Early in the development of its graduate training program, the School recognized that men and women engaged in research should be as free as possible of the administrative duties involved in sponsored research. In 1959, therefore, the Research Laboratories for the Engineering Sciences (RLES) was established and assigned the administrative responsibility for such research within the School.

The director of RLES—himself a faculty member and researcher—maintains familiarity with the support requirements of the research under way. He is aided by an Academic Advisory Committee made up of a faculty representative from each academic department of the School. This Committee serves to inform RLES of the needs and perspectives of the research program.

In addition to administrative support, RLES is charged with providing certain technical assistance. Because it is not practical for each department to become self-sufficient in all phases of the supporting technology essential to present-day research, RLES makes services available through the following support groups: Machine Shop, Instrumentation, Facilities Services, Publications (including photographic facilities), and Computer Terminal Maintenance.

(9) A Technical Report,

(6) INVESTIGATION OF ELONGATION AND ITS RELATIONSHIP TO RESIDUAL STRESSES IN BORON FILAMENTS.

Submitted to:

Office of Naval Research
800 N. Quincy Street
Arlington, VA 22217

(10) Franklin E. Wawner, Jr.
J. W. Eason Robert A. Johnson

Submitted by:

F. E. Wawner
Research Professor

J. W. Eason
Graduate Research Assistant

Robert A. Johnson
Professor

(14) UVA/525322/MS79/102, TR-2

Department of Materials Science
RESEARCH LABORATORIES FOR THE ENGINEERING SCIENCES
SCHOOL OF ENGINEERING AND APPLIED SCIENCE
UNIVERSITY OF VIRGINIA
CHARLOTTESVILLE VIRGINIA

(15) N0014-76-C-0694

(12) 103p.

Accession For	
NTIS GRA&I	☑
DDC TAB	☐
Unannounced	☐
Justification	
By	
Distribution/	
Availability Codes	
Dist	Avail and/or special
A	

Report No. UVA/525322/MS79/102 Copy No. 6

(11) September 1979

401 761

jb

ABSTRACT

Elongation in boron filament during fabrication was investigated and found to be as great as 16% under certain conditions. It was also found to obey a relatively simple empirical relationship which yielded effective activation energies. A model for the elongation was proposed, and a computer program was designed to simulate the deposition and elongation of boron on a tungsten wire substrate. Internal residual stress distribution of boron/tungsten filament were also generated by the computer program. Good agreement was found between the proposed model and experimental results. Negative elongation (contraction) of boron filament was observed during annealing and found to be dependent upon the concentration of oxygen present in the annealing atmosphere. The contraction was also found to be the result of void formation at the core-boron sheath interface. The contraction obeyed an empirical relationship, which represented an exponential decay toward equilibrium from a non-equilibrium state and an effective activation energy was determined for boron/tungsten filament.

79 09 27 011

SECTION I

INTRODUCTION AND BACKGROUND

Boron filaments are perhaps one of the most technologically important developments in the materials industry in many years. The high specific strength and modulus of this material makes it ideal as a reinforcement for organic and metal matrix composites. Many applications for the material can be envisioned, however, there has been a certain reluctance by designers and manufacturers to utilize boron composite materials primarily because of their high cost. There are limited applications today, particularly in the aerospace industry, where boron composites are cost effective. In the large part however they have been excluded from incorporation into specific hardware items because of the stigma of high cost. Conventional materials are then used without long-range considerations of cost savings due to improved performance and service life.

Several factors can be cited which would reduce the cost of the filaments and hence the ultimate composite cost, the primary one of which is volume. But it is difficult to create a volume market without first reducing the price to a cost competitive level. Based on this premise, a secondary factor to reduce the cost of the filament is to increase production speeds. It is physically possible to increase production speeds of boron filaments

by 2-3 times using existing manufacturing equipment and techniques; however, the filament obtained is of inferior quality having, generally, a low tensile strength making it unacceptable for existing composite specifications. The reason for the low tensile strength has been attributed to an internal defect called the "crack tip" mode of failure and is believed to be related to an undesirable residual stress distribution in the boron filament. This is based on the fact that the low tensile strength is occasionally accompanied by spontaneous splitting of the filament. Consequently, if one could understand the residual stress distribution in boron filaments, its relationship to facture of the filaments, and what factors influence it, then it might be possible to determine techniques to alter the residual stress pattern to a more favorable configuration. This would lead to faster production speeds and considerably lower cost boron filament.

Several limited studies have been conducted on residual stresses in boron filaments[1-7]. The essence of these studies was to determine the configuration, magnitude and apparent causes of the stresses in the filaments. Virtually nothing has been done to relate specific process conditions or fundamental material properties to unfavorable stress distributions. Unfortunately, this area of research was ignored when accelerated emphasis was placed on fabricating

and studying the filament in composites. The results of the above studies were all basically in agreement showing the outer surface layers being in residual compression, the layers of boron next to the tungsten boride core being in residual tension and the core itself being in residual compression. Figure 1 is a schematic diagram depicting the typical residual stress configuration in the boron layer for a filament produced on a tungsten and a carbon substrate. In general, the reported magnitudes for the stresses vary depending on the techniques used for measurement, however, all are within reasonable agreement.

The primary causes of the residual stresses were attributed to: thermal expansion mismatch between deposited boron and the boride core; volume expansion within the core due to diffusion and reaction to form borides; quenching in the mercury electrode at the exit end of the reactor; and elongation in the boron during deposition. Both boron filaments produced on tungsten and carbon substrates contain residual stresses, however, filament produced on carbon do not appear to give as high values as boron on tungsten. This is probably due to the fact that there is no diffusion and reaction and hence volume expansion in the core region eliminating this cause.

Of the aforementioned contributors to the residual stresses in boron filaments, it is felt that boron elongation

during deposition is perhaps the predominant cause of unfavorable residual stress patterns when attempting to increase production speed. Talley[8] first detected the phenomena when he noted that boron deposited on a tungsten substrate elongated by 10%. More recently other investigators[9,10] have conducted a broader study of the effect while attempting to deposit boron on carbon monofilament substrate. It was observed that the boron elongated sufficiently to break the carbon substrate. This is due to the fact that the boron layer formed a sufficiently strong bond with the carbon substrate and the elongation during deposition exceeded the strain to failure of the non-elongating carbon monofilament, causing fracture. Fracture of the carbon substrate created local electrical discontinuities and hence hot spots which gave rise to crystalline boron of very low tensile strength.

Measurements showed that boron elongation was primarily dependent on deposition temperature being the greatest for the low temperature end of the deposition range (i.e. approximately 2.5% elongation at 1000^{o}C versus 1% elongation at 1200-1300^{o}C at a diamter of 2 mils). Other factors such as reactant gas composition, selected impurity additives or tension of the substrate appeared to have little or no effect. A technique was devised to cirvumvent this phenomenon by pre-depositing a thin layer of pyrolytic

graphite which did not bond with the carbon monofilament thereby allowing the boron to slide and rearrange during elongation.

Boron elongation, in general, is one of the least understood fundamental properties of the material. It is certainly a prime contributor to the residual stress distribution in the as produced filament and this stress distribution has a strong bearing on tensile and transverse strengths (splitting).

Along these same lines, observations have been made by Soviet scientists[11,12,13] which may also be strongly related to elongation and residual stresses in boron filaments. These studies showed that annealing the filaments at approximately 300^{o}C for short times increased the tensile strength by 12%. This increase was accompanied by a decrease in flexural strength which was not understood. Of interest is the fact that the material displays an internal friction peak (a relaxation maximum) at approximately the same temperature. Also, it was noted that there is anomalous behavior in the thermal expansion characteristics and in resistance in the filaments in this same temperature region. These observations along with boron elongation may be influenced by or related to the anelastic behavior displayed by boron filaments and recently described by DiCarlo[14]. Some evidence in the present program suggests that there is a

relationship. All of these appear to be fundamental phenomena which are probably controlled by a structural rearrangement in the material and have a possible relationship with the elongation and residual stress phenomena.

The steps taken to minimize the influence of boron elongation on carbon substrate were really circumventing or ignoring the basic problem in order to achieve a viable product. The procedure to pre-deposit the PG layer while successful has its limitations and adds to the cost of producing the filament. This emphasizes the purpose of the present work that if we can understand the fundamental property of elongation and hence residual stresses in boron then there may be certain measures one can take to eliminate or control it.

The primary objective of this investigation is to perform a fundamental study on elongation in boron produced by chemical vapor deposition in an attempt to understand the basic nature of this phenomenon. It is then planned to determine what factors influence boron elongation and how it is related to the elastic properties and the ultimate residual stress distribution in as produced boron filaments. Using these results it will be possible to investigate techniques to minimize the elongation which will possibly lead to faster filament production speeds and lower cost filament.

EXPERIMENTAL PROCEDURE

A typical boron production reactor is schematically shown in Figure 2. The reaction to form boron filaments is carried out by the hydrogen reduction of boron trichloride in the manner described by the equation

$$2BCl_3 + 3H_2 \xrightarrow{\text{heat}} 2B + 6HCl.$$

The substrate wire, typically 13 micron tungsten, or 36 micron carbon in pulled through the chamber by a substrate takeup motor and is heated electrically to the desired temperature (1000 - 13000^{o}C). Mercury serves as electrical contacts as well as gas seals in the chamber. A mixture of the reactant gas is passed through the deposition chamber at positive pressure where it contacts the heated substrate wire and deposits boron. Also shown in this figure is the temperature profile assumed by boron filament on tungsten while it is being produced. The highest temperature along the profile is called the deposition of "hot spot" temperature and is normally located just a few inches below the entrance end of the reactor. The temeprature at the exit end of the reactor is 200-300^{o}C lower than at the "hot spot" and is due to a resistance decrease in the filament as the diameter increases (current is maintained constant through a filament during production). Hence one can see that "normal" as produced boron (on tungsten) filaments are deposited over a rather severe temperature gradient which considering the

contribution of boron elongation leads to a complicated residual stress situation.

In spite of the apparent undesirability of the temperature profile, it is this profile that has produced the highest quality filament. Speeding the process up by creating a uniform temperature profile in the reactor by means of auxiliary VHF heating or by other techniques (of a proprietary nature) have lead to poor quality filament that predominantely fail as a result of the characteristic "crack tip" mode of failure, representative of abnormal residual stresses.

The program being conducted at UVA is to produce boron filament by chemical vapor deposition using a static reactor. Using this type reactor will eliminate many of the variables encountered in a continuous process and allow much greater control over growth of the filament and consequently greater ease of observation and recording of the growth and elongation process. A very important factor using this type reactor will be the ability to achieve and maintain a uniform temperature along the length of the filament during boron growth.

Elongation measurements are made using the device constructed during the program and shown schematically in Figure 3. The basic concept is one of a change in inductance of a coil located in a bridge circuit. A small steel rod

is attached to the substrate and positioned in the coil. The meter is then set at zero by a balancing resistor. As the filament elongates during growth, readings can be taken from the meter or traced by a recorder for a permanent record. The substrate is heated resistively by a DC power supply and the temperature measured by a Milletron Ratioscope.

Substrates used to date in this study have included tungsten of diameters 5, 13, 18, 33, 38 and 43 microns and carbon of 36 microns in diameter. The carbon substrate was coated with a thin layer (approximately 1 μ) of pyrolytic graphite to minimize "light bulbing".

Primary deposition variables investigated have been deposition temperature, filament tension, substrate diameter and doping (impurity addition).

In addition to elongation measurements the filaments were subjected to a series of characterization experiments to define structural and microstructural phenomena. A Philips 400 analytical electron microscope was used to obtain electron micrographs and electron diffraction patterns from inner and outer portions of the filaments. Filaments subjected to electron microscopy were appropriately thinned (either from the outer surface to the inner surface or vice versa) using an ion micromilling instrument (Commonwealth Scientific Model III).

Experiments to measure the anelastic effect in the filaments were made using the previously described elongation measurement device while heating to various temperatures in a hydrogen, nitrogen and argon atmospheres.

SECTION II

EXPERIMENTAL RESULTS AND DISCUSSION

Boron/Carbon Chemical vapor deposition of boron by hydrogen reduction of boron trichloride onto a heated substrate generates characteristic axial residual stress patterns (see Figure 1). Understanding the mechanisms that develop these stresses is essential to the comprehension and control of the mechanical and physical properties of boron filament. One of the major factors believed to be involved with the development of the residual internal stresses is the elongation of boron during deposition. Mehalso[15] studied the deposition of boron onto a carbon monofilament substrate and observed the filament elongation. Boron on carbon filament elongation was measured and found to be great enough to cause fracture of the carbon substrate.

Figure 4 shows a plot of elongation vs. deposition time for different runs using a carbon substrate. One curve depicts a run at a deposition temperature of 1250°C, which utilized "plant BCl_3" in the reactant gas. The term "plant BCl_3" was used to identify boron trichloride which was recovered and recycled from other deposition runs, and it was known to contain small amounts of diborane (B_2H_6). Also shown in Figure 16 is a curve of a run at a deposition temperature of 1250°C, which used "depleted BCl_3" in the reactant gas mixture. "Depleted BCl_3" refers to boron trichloride which contains no diborane (B_2H_6) and corresponds

to the boron trichloride as received from the commercial supplier. It was noted that a small difference in elongation is seen between the two types of BCl_3. However, the difference was shown to be insignificant when compared to the effects of deposition temperature. By addition of weight attached to the substrate, an increase in tension was imposed on the filament. The effect of increased tension on elongation is also shown in Figure 4. This change in elongation seems reasonable since the phenomenon of elongation is such that a tensile stress is transmitted to the substrate, and if the tensile stress is increased by an outside influence, then one should expect an increase in the elongation.

Deposition temperature has a most interesting effect on the elongation of boron/carbon filament. As stated previously, the elongation of the boron during deposition is sufficient to cause fracture of the carbon substrate. If the deposition temperature is high enough, then creep can occur in the carbon substrate allowing it to elongate with the boron sheath, thus minimizing fracture of the core. At lower deposition temperatures, the creep rate is not sufficient to prevent fracture of the core.[15] The result is a phenomenon called "light bulbing." An electrical discontinuity arises at the region of core fracture, and the increased electrical resistance causes an increase in filament temperature at the discontinuity. Rapid deposition and growth of boron occurs at these points and is generally

crystalline. Figure 5 shows deposition runs of boron/carbon at two different temperatures. It can be seen from these curves that creep in the carbon substrate is not sufficient to prevent fracture at 1200°C; whereas it is great enough at 1250°C for the core to conform with the elongating boron. These two curves show that fracture of the carbon core occurs at about 1% strain. After fracture the elongation increased rapidly since the constraint to the elongation by the substrate was reduced. The final elongation was also dependent on the number of sites where fracture of the substrate occurred, and this effect is shown in the difference of the elongation curves for "some light bulbing" and "much light bulbing." This "light bulbing" effect can be reduced somewhat, but not eliminated, by coating the carbon monofilament with a thin (≈1 μm) layer of pyrolytic graphite (PG). An analysis of boron elongation with respect to deposition temperature cannot easily be made because of this "light bulbing" phenomenon.

Figure 6 shows that the final radius squared is linear with time at a high deposition temperature for boron/carbon filament. This graph implies diffusion rate limited kinetics,[15] and it allows one to calculate the radius (or diameter) of the filament at any given time during deposition.

A plot of elongation (A) vs. final diameter of the filament is shown in Figure 7. Several different runs,

using "depleted" and "plant" BCl_3, were averaged together. The resultant curve somewhat resembled a parabola, implying that the elongation may be linear with respect to the radius squared. A plot of A vs. R^2 is shown in Figure 8, and it was noted that the elongation was linear with R^2 for the early stages of deposition and non-linear for the later stages of deposition. This result suggests that the elongation is a more complex function of the radius of the boron filament than a simple dependence on the cross-sectional area of the boron deposit.

An important experimental result was found by using a carbon substrate. Elongation measurements were made during deposition of boron on carbon at a temperature above the value at which a crystalline boron deposit is formed (>1300°C). It was found that a negative elongation of approximately 1% occurred at these temperatures. A crystalline deposit implies that the boron atoms are deposited at definite lattice sites, and that little, if any, rearrangement of the lattice occurs after deposition. This is in support of the model which is discussed later.

Boron filament with a carbon monofilament or a pyrolytic graphite coated carbon monofilament substrate are at present not widely used in the commercial market, and are still in the developmental stage of production.[16] Consequently, this investigation concentrated on the more widely used boron/tungsten filament for evaluation of the elongation

phenomenon.

Boron/Tungsten Talley[8] first observed the elongation of boron on tungsten to be approximately 10%. Little has been reported since to quantitatively characterize the elongation of boron, except for work performed by Diefendorf [17] and Mehalso.[15] Conclusions from these studies indicate that boron elongation is dependent upon: (1) deposition temperature; (2) substrate type and size; and, (3) amount of boron deposited.

An elongation vs. deposition time plot is shown in Figure 9 to give the reader an idea of how the elongation proceeds in real time during a typical deposition run. The substrate used was a 13 μm (0.5 mil) diameter tungsten wire, which is the standard substrate used commercially. The total gas flow in the static reactor was approximately 1 liter/min and was a 60% H_2 - 40% BCl_3 stoichiometric mixture. The deposition temperature was 1200°C. By changing the composition or the total gas flow, one could alter the deposition rate of boron, and hence, change the shape of the curve. A change of the dependent variable (i.e., time) to the final radius of the boron filament results in a more fundamental relationship, so that the only parameters which have a significant effect on the shape and slope of the curve are: (1) deposition temperature; and, (2) substrate.

Figures 10 and 11 show the effect of deposition temperature on boron elongation vs. final radius of boron/

tungsten filament. The final elongation was found to increase with increasing deposition temperatures for filaments with small radii (i.e., R <31 μm). For filaments with large radii (i.e., R >31 μm), the elongation was found to decrease with increasing deposition temperature. The temperature dependence experiments were all carried out using 13 μm (0.5 mil) tungsten wire as a substrate. The fact that the elongation increases with increasing temperature for small radii filaments (R <31 μm), and decreases with increasing temperature for larger radii filaments (R >31 μm), most probably results from the elongation phenomenon being dominated by the volume expansion of the tungsten core during the early stages of deposition. After the core is completely developed into W_2B_5 and WB_4, the elongation is then primarily due to the elongation of the boron sheath. This effect is more clearly seen in Figure 10, which shows the difference in elongation vs. final radius between a set of deposition experiments performed at 1200°C, and a set performed at 900°C. Figure 11 shows the results of experiments carried out at intermediate temperatures (1000°C and 1100°C). An interesting result from the four different temperature curves in Figures 10 and 11 is a common point which occurs at an elongation of 6.5% and a filament radius of 31 μm. The experimental data had sufficient scatter as to preclude any speculation about the common point. However, the four different temperature curves do begin to diverge from this

point. The lower final elongation at the higher deposition temperatures could be attributed to the fact that at higher temperatures atomic mobility was increased, allowing the atoms to form a more dense, lower energy configuration. Indeed, if the deposition temperature is raised above 1300°C, crystalline boron forms in the deposit.

The curves used to fit the experimental data in Figures 10 and 11 are least squares fits of an empirical relationship. The general form of the elongation curves can be approximated by the equation:

$$A = A_0 \left(\frac{R - r_c}{R + r_c} \right)^n \qquad (3)$$

where

$A \equiv$ elongation of boron filament

$R \equiv$ radius of boron filament

$r_c \equiv$ radius of substrate

A_0 and n are fitting parameters.

Differentiation and rearrangement of equation (3) results in another relationship:

$$\frac{dA}{dR} = \frac{\frac{n}{2r_c} A}{R^2 - r_c^2}. \qquad (4)$$

This implies that dA/dR increases linearly with A, and is inversely proportional to the cross-sectional area of the deposited boron. The fitting parameters A_0 and n listed in Tables 1 and 2 show a regular variation in the deposition

temperature-dependence set of runs, but are rather irregular in the filament core size variation set of runs.

Figure 12 is an Arrhenius plot of the two fitting parameters A_0 and n for the deposition temperature variation set of experiments, which were performed using the standard 13 μm (0.5 mil) diameter tungsten wire as a substrate. The reader may note the remarkable regularity of the values of A_0 and n, which gives strong support to the validity of equation (3) as the analytical form of boron/tungsten filament elongation. A least squares fit to the data in Figure 12 yields the result:

$$n = 0.097e^{0.33/kT}$$

and,

$$A_0 = 1.31e^{0.27/kT}.$$

This result implies two effective activation energies of 0.33eV and 0.27eV. These activation energies seem quite low for an atomic migration phenomenon and no definite explanation of these energies can be offered. The elongation phenomenon clearly involves the diffusion and reaction of boron with tungsten, but there is also a process occurring in the boron itself, as evidenced by the results of elongation experiments using a carbon core.

Figures 13, 14 and 15 show the results of the core size variation set of experiments. The substrates used were 5.2 μm (0.2 mil), 17.8 μm (0.7 mil), 33 μm (1.3 mil), 38 μm (1.5 mil) and 43 μm (1.7 mil) diameter tungsten wires,

supplied to the author by AVCO Specialty Materials Division. All experiments were conducted at a constant flow rate and BCl_3 - H_2 mixture of 1 liter/min and 40% - 60% respectively. A deposition temperature of 1200°C was also used for all runs. A least squares fit of equation (3) was used to generate the curves shown in Figures 13, 14 and 15, and values of the fitting parameters A_0 and n are shown in Table 2. The irregular variation of the parameters A_0 and n were presumably the combined result of possible differences in experimental conditions and differences in the microstructure and surface texture of the various sized tungsten substrates, which affect these parameters in an unknown way. The experimental results, given in Figures 13, 14 and 15 show the profound effect that the substrate size has upon the elongation of the boron/tungsten filament. The difference in the filament elongation can be explained by the difference in boridization of the tungsten core. For the small diameter (5.2 μm) tungsten substrate, the distance which the boron must diffuse through the core to achieve complete boridization is obviously smaller than for a large diameter (43 μm) substrate. It has been shown[18] that a 13 μm (0.5 mil) diameter tungsten substrate was completely borided when subjected to similar deposition conditions as were used in the present set of deposition experiments; therefore, one may assume that a 5.2 μm diameter tungsten substrate would be completely borided under the same conditions. The presence

of unreacted tungsten in the core of a B/W filament would tend to restrain the expansion of the outer regions of the core, thereby restraining the elongation of the entire filament. This type of behavior is reflected in the results shown in Figures 13, 14 and 15.

Boron/Boron Several experiments were conducted by depositing boron on a commercially produced 102 μm (4 mil) diameter B/W filament. The result of these experiments is shown in Figure 16. It was noted that this elongation curve was an extension of the 1200°C elongation curve shown in Figure 10. This result was reasonable since the B/W filament used as a substrate for the experiments shown in Figure 16 also had a 13 μm (0.5 mil) tungsten substrate. Also shown in Figure 16 are results of deposition experiments using a 142 μm (5.6 mil) B/W filament as a substrate. Again, this curve can be seen to be a continuation of the 1200°C curve of Figure 10. The data for this 142 μm B/W curve was submitted to the authors by AVCO Specialty Materials Division. These results implied that the elongation phenomenon was a continuous function of the filament radius whether the deposition was interrupted and performed in steps, or was continuous. Figure 16 shows the results of boron elongation only as opposed to filament elongation influenced by core development.

Doping Experiments A number of experiments were performed by introducing an additional chemical vapor or gas into the standard boron deposition gas mixture. Three

different dopant gases were used: tungsten hexaflouride (WF_6); silicon tetrachloride ($SiCl_4$); and methane (CH_4).

Tungsten doping of the boron deposit was achieved by including tungsten hexaflouride in the deposition gas mixture. Preliminary experiments indicated that small additions of tungsten hexaflouride to the deposition gas mixture had no significant effect on the elongation of boron filament. However, an interesting experimental result was revealed from x-ray diffraction measurements. Boron and tungsten were simultaneously deposited onto a 13 μm (0.5 mil) tungsten substrate. The flow rate ratio of WF_6:BCl_3 was estimated to be 1:1, and the deposition temperature was approximately 1200°C. A cross-sectional micrograph (SEM) of the tungsten-boron filament is shown in Figure 17, and the x-ray diffraction analysis of this filament is given in Table 3. Noted were the highly convoluted surface and the presence of regularly spaced radial cracks in the deposit. The filament was quite brittle and had a low tensile strength. The interesting result was that the x-ray diffraction measurements revealed the deposit to be tungsten diboride (WB_2), an infrequently observed Tungsten boride phase. Woods et al[19] have reported the formation of WB_2 on a boron filament by heating the filament to 800°C for 30 minutes in a reduced pressure atmosphere of argon and WF_6.

Silicon was used as a dopant in the boron deposition by the addition of silicon tetrachloride ($SiCl_4$) vapor to the

reactant gas mixture. The addition of silicon tetrachloride vapor was accomplished by bubbling hydrogen through $SiCl_4$ liquid at room temperature. A gas washing bottle was used to contain the $SiCl_4$ liquid. Hydrogen was bubbled through the liquid by means of a porous glass frit submerged in the $SiCl_4$, in order to maximize the amount of vapor carried over into the deposition chamber. The flow rate of the carrier gas (H_2) was recorded for the different sets of deposition experiments. A 13 μm (0.5 mil) tungsten substrate was used for the silicon doping experiments. The elongation of the filament was recorded, and the results are shown in Figure 18. The numbers in parentheses shown with the data points are related to the flow rate of the hydrogen carrier gas and the actual values are: (0) = 0 liters/min; (40) = 0.12 liters/min; (60) = 0.19 liters/min; (80) = 0.3 liters/min; (120) = 0.54 liters/min. No definite effect on elongation of the filament was seen from the silicon doping experiments, but analysis of x-ray diffraction results indicated that silicon did become incorporated in the boron deposit. As a matter of fact at the maximum concentration of $SiCl_4$ (0.54 1/min) the strongest two diffraction peaks for SiB_6 were detected in the deposit.

Carbon was also used as a dopant in several boron deposition experiments. Methane (CH_4) was used as the source of carbon in the different runs, and pyrolytic graphite (PG) coated carbon filament was used as a substrate. Results from these experiments are shown in Figure 18. The numbers in parentheses shown with the data points correspond to the flow rate ratio of BCl_3 to CH_4 (i.e., (10) = 10:1 BCl_3:CH_4, (20) = 20:1 BCl_3:CH_4, etc.). The increase of the flow of methane (CH_4) in the deposition gas mixture was found to have a definite influence on the elongation of the filament. As the amount of CH_4 was increased, the elongation as a function of the radius of the filament decreased. This was a very important result. Unlike tungsten and silicon, carbon can substitutionally enter the boron lattice and form a variety of solid solutions and crystalline compounds. X-ray diffraction measurements were made on each set of carbon doping experiments. A qualitative examination of these x-ray patterns reveals changes in width of the primary halos of amorphous boron and appearance of crystalline lines at the higher concentrations of methane in the deposition gas. These analyses show that discrete carbon-boron compounds are not detectable in the filament until the BCl_3:CH_4 flow ratio reaches a value of approximately 20:1. At the 20:1 ratio a very very weak line was observed and found to correspond to the strongest line of the x-ray diffraction

pattern of boron carbide (B_4C). Increasing the methane content of the reactant gas mixture to a BCl_3:CH_4 ratio of 15:1 revealed an interesting result. The increase in carbon content of the deposit resulted in the formation of a boron-carbon compound with a molecular formula of $B_{48}B_2C_2$,[20] ($B_{25}C$). $B_{13}C_2$, which closely resembles B_4C, was also detected, although the line was very weak. An anomalous line appeared in the diffraction pattern of this set of filament and it was identified as the strongest line of an impure graphite. This line was possibly due to small islands of graphite formed in the deposit with boron present as an impurity. Further increase of the methane flow corresponding to a BCl_3:CH_4 ration of 10:1 resulted in filament which exhibited greater crystallinity. Analysis of the x-ray diffraction pattern showed that lines pertaining to $B_{25}C$ were the predominant lines. A small amount of $B_{13}C_2$ also appeared to be present.

These results show that by doping the deposition gas mixture (BCl_3-H_2) with methane, carbon is included in the boron deposit and forms crystalline boron-carbon compounds plus small amounts of graphite with boron as an impurity. Elongation was shown to decrease as the amount of carbon in the deposit was increased. The increase of carbon content in the deposit was also accompanied by an increase

in crystallinity, as evidenced by the diffraction patterns. These two factors seem to imply that an increase in crystallinity results in a decrease in the elongation of boron. This statement must be qualified; the incorporation of silicon and tungsten into the boron also increases the crystallinity of the deposit. However, silicon and tungsten do not substitutionally enter the boron lattice, and an expansion is involved in the formation of three dimensional cages of boron atoms around the metal atoms in metallic borides.[21] Nevertheless, the experimental results presented here support the model for elongation discussed below.

TRANSFORMATION MODEL

Considering the phenomenon of elongation and the experimental data that has been presented, the question remains as to the basic source of boron elongation. When a tungsten substrate is used for the production of boron filament, the diffusion of boron into the tungsten and the resultant expansion is clearly a major contributor to the elongation that is observed. However, when a carbon substrate is used, there is no significant diffusion of boron into the carbon, yet the elongation of the boron is sufficent to fracture the substrate. Also, when depositing boron onto large diameter boron filament with the core already developed,

one observes elongation. Consider the deposition process, mentioned earlier, that is involved in the fabrication of a boron filament. Boron trichloride and hydrogen react at the surface of the substrate, boron atoms are deposited onto it, and hydrogen chloride (HCl) diffuses away from the surface of the substrate. There are other by-products and intermediate species formed by partial reduction of the BCl_3 by H_2, such as $HBCl_2$ and B_2H_6, but these are not the predominant reaction products and the boron is primarily deposited as individual atoms. Consider also, that is has been shown[22-28] that the B_{12} icosahedron is the integral subunit of structure found in all the known polymorphs of boron. While it is not inconceivable for B_{12} icosahedra to form in the gas phase and then deposit on the surface, it seems improbable that this is the actual deposition process which takes place during the fabrication of boron filament. A model can be developed as follows: the assumption was made that nearly all the boron atoms were deposited individually and in a random configuration. Each layer of atoms deposited were continually being covered by fresh deposit. These buried atoms transformed, at some rate, from a random distribution of individual atoms into a random distribution of B_{12} icosahedra. The edge length of the B_{12} icosahedra is 1.78 Å. By treating the boron atoms as hard spheres, the volume of each boron atom, using 1.78 Å/2 as the radius of the boron atom, is V_B = 2.95

$\mathring{A}^3$. The volume of twelve boron atoms would then be V_{12_B} = 35.43 $\mathring{A}^3$. If one approximates an icosahedron as a sphere, then the volume of a B_{12} icosahedra would be $V_{B_{12}}$ = 72.12 $\mathring{A}^3$. This result implies a volume expansion when transforming from isolated atoms into icosahedra. In fact, there would be a volume expansion resulting from this particular transformation for an isolated atom packing factor as low as 0.50.

In view of the atomic volume consideration given above, the following model is presented to give a qualitative explanation to the elongation upon deposition of amorphous boron on tungsten:

(1) as boron is deposited, it forms an amorphous layer of boron atoms on the surface;

(2) this amorphous layer of atoms transforms to an amorphous layer of icosahedra with a resultant volume expansion;

(3) if the stress becomes sufficiently large at any point in the boron sheath, the boron deforms to limit the stress to a given maximum value;

(4) boron diffuses into the tungsten core;

(5) the tungsten-boron solution transforms to tungsten borides with a resultant volume expansion;

(6) if the stress becomes sufficiently large at any point in the core, the diffusion - transformation process is retarded;

(7) the integrated axial stress across a cross-section of the fiber is zero.

A computer program was designed to check whether this model could yield a rough quantitative comparison with the experimental results. Since approximations had to be made in this model and it contains a number of unknown parameters, detailed fitting was not carried out.

Runs were made with core diameters of 4.8, 12 and 36 μm. It was assumed the radius increased linearly with deposition time at a rate of 48 μm/min, and that the boron would reach the center of the 12 μm diameter core sample in 1 minute. Young's modulus was taken as the same in the sheath (E) and throughout the core (E_c) (whether transformed or not). It was also assumed the transformation of the deposited boron, if it was not constrained, would proceed as (see Appendix):

$$\left[1 + (f - 1)\ (1 - e^{-kt})\right] \qquad (5)$$

where

t ≡ the time at which the boron layer was deposited

f ≡ expansion factor

k ≡ a rate constant.

This function varied from 1 to f as t goes from 0 to infinity. The expansion factor (f) was taken as 1.1 and k as 0.37/sec, so that the transformation was half complete by the time a deposited layer was covered by 1.5 μm of additionally

deposited boron. The core expansion factor was taken as 1.2, and the maximum elastic strain permitted in the core or the boron sheath was taken as (E) = 0.3%. Results from these computer runs are shown in Figure 19 and are the result of the equation:

$$X_n = \frac{\frac{1}{2}\left[R^2 + \left(\frac{E_c}{E} - 1\right) r_c^2\right]}{\frac{E_c}{E}\int_0^{r_c} \frac{rdr}{1+S\left(\frac{R-r_c}{\alpha} - \frac{r_c-r}{\beta}\right)\left(f_c-1\right)\left[1-\exp\left(K_c\left(\frac{R-r_c}{\alpha} - \frac{r_c-r}{\beta}\right)\right)\right]} + \int_{r_c}^{R} \frac{\ell(r_c)}{\ell(r)} \frac{rdr}{\left[1 + (f-1)\ (1-e^{-k/\alpha(R-r_c)})\right]}} \quad (6)$$

Also shown in Figure 19 are curves generated from the empirical fit discussed earlier. Certainly, the correct behavior is seen, as compared to the experimental results shown in Figures 13, 14 and 15.

The model presented in this investigation assumes that an expansion takes place in the deposited boron sheath as a result of the transformation from isolated boron atoms into B_{12} icosahedra. With constraints on the expansion, imposed by the surrounding material, a state of compression would develop in the transforming layer of boron atoms (at some filament radius R_i), and this state of compression would exert a tensile stress onto the underlying material. As deposition continued, the layer at R_i would successively be

buried deeper and deeper by additional layers of boron. Each layer would develop its own internal state of compression which in turn would exert a tensile stress onto the underlying layers of material. After some thickness, $R > R_i$, was reached, the initial layer considered (R_i) would have its state of compression somewhat relieved. When the radius of the filament (R) reached a value sufficiently larger than R_i, the state of compression initially developed in R_i would be completely relieved. With further deposition, the layer designated as R_i would exhibit a progressively increasing state of tension until the tensile strain reached a critical value, which would result in either fracture or non-elastic deformation. Axial residual stress distributions were generated by the computer model and the results were of the same general form as that determined experimentally[2] (Figure 1). In the smaller two samples (4.8 μm and 12.0 μm), the core was under compression near the maximum allowed stress, the inner portion of the sheath was under tension near the maximum allowed stress, and the outer portion of the boron sheath was under compression near the maximum allowed stress. The computer model axial residual stress distribution for the largest core size (36 μm) is shown in Figure 20, and it

was noted that the center portion of the core was under tension, since diffusion and resultant transformation to tungsten boride had not taken place. The change from tension to compression, in the boron sheath, occurs more abruptly in the model than reported experimentally[2] (Figure 1), but at about the same radius. A possible reason for the difference between the experimentally determined axial stress distributions and the computer model axial stress distributions is that the model does not take into account the thermal contraction that takes place after deposition is completed. The complete mathematical development of the model presented above is given in the Appendix.

Annealing Experiments The fact that boron displayed anelastic behavior indicated that it might show some recovery from the original elongation. Originally, boron filaments were annealed in different inert atmospheres (N_2, Ar, H_2). A contraction of 1.3 to 1.9% was observed for all gases used, following annealing at 900°C for 10 minutes. Annealing was also conducted in a vacuum (10^{-7} Torr), and when crystallization did not occur, no contraction was observed. Examination of the data suggested a common mechanism involved with the gaseous environments. It is known that the presence of water vapor has undesirable effects on boron growth during the deposition process, and care was taken to ensure that all gases were dry before entering the system. The common factor believed to be involved was trace amounts of oxygen present

in the annealing environments. Consequently, experiments were carried out in dry air to accelerate the mechanism. Boron filaments with different histories were used, and the results are shown in Figure 21. The different filaments were: (1) standard production 102 μm (4 mil) diameter B/W filament stored at room temperature for 4 years; (2) standard production 102 μm (4 mil) diameter B/W filament recently made; (3) standard production 107 μm (4.2 mil) diameter B/C filament; and (4) standard production 107 μm (4.2 mil) diameter B/C filament etched to 74 μm (2.9 mil). Figure 21 shows that all of the boron filaments contract upon annealing. The temperature was kept constant at 900°C. After 10 minutes, the standard production B/W filaments contracted by 1.7%; whereas, the B/W filaments that had been stored for 4 years contracted somewhat less (1.4%), indicating some recovery, even at room temperature. Boron on carbon filaments contracted to a lesser extent, approximately 1%, but this should be expected because of the difference in magnitude and distribution of the residual stresses[2] and less original elongation as compared to B/W filament. Similar B/C filaments that had been reduced in diameter by etching, thereby redistributing residual stresses in the filaments, contracted by only 0.3%. Etching the filament removed the compressive layer on the outer surface of the filament, allowing the tensile stresses in the inner portion of the

boron sheath to relax. This, in itself, permitted some contraction in the filament, which reduced the contraction resultant from annealing.

All annealing experiments that were previously conducted resulted in coating the inside walls of the chamber with a white film that physically resembled boron oxide (B_2O_3), (i.e., it was soluble in hot water and slightly soluble in ethyl alcohol, and hexagon crystals were observed). Therefore, oxygen was considered the most likely gaseous species in the annealing environment responsible for the relatively large contractions observed. Research purity nitrogen (guaranteed to contain <1 ppm O_2) was used as a carrier gas, while small amounts of dry air were added to the flow to change the oxygen content of the annealing atmosphere. Figure 22 shows the results of these experiments. The solid circles shown on the graph represent individual experiments, except for the one corresponding to 0% oxygen. Several runs were made in this pure nitrogen atmosphere for periods of time exceeding 20 minutes (1200 sec) in order to accurately define the result. The solid line represents an exponential decay toward equilibrium, which will be discussed later. The contractions observed were found to be the result of oxidation of boron at the surface of the filament. Boron oxide is volatile at the temperatures used when annealing the filament, as evidenced by the film of boron oxide on the chamber walls, so that this

oxidation was an effective method of removing boron from the surface of the filament. A micrograph of the surface of an annealed boron filament is shown in Figure 23a. It was noted that the surface was considerably smoother than that of an as-produced boron filament but the original diameter did not change.

The observation of voids in boron filament, both in metal matrices[29-32] and in the present work, suggests that the mechanism of void formation is related to the diffusion of boron atoms outward to the surface and vacancy diffusion inward to the core - sheath interface. A critical factor in understanding all diffusion phenomena is dependence on temperature. Many boron filaments were annealed in dry air at constant periods of time, (300 sec) at temperatures ranging from 800°C to 1200°C. The lower limit of 800°C was imposed by the optical pyrometer and the upper limit of 1200°C was due to the transformation of amorphous boron to a crystalline phase or phases. The results from these experiments are shown in Figure 24. The solid circles on the graph are the mean values of contraction with bars representing the standard deviation for each set of experiments. The solid line represents another exponential decay (see Equation 8), which allows for contraction to take place, even at room temperature. An interesting point to note is that the maximum slope of this curve occurs in the region between 900°C and 1000°C. Figure 23b shows that macroscopic voids were first observed in this temperature range at 300 seconds

annealing time.

Figures 22 and 24 both exhibit an exponential decay toward equilibrium. This is common in nature; (radioactive decay, amplitude of vibration of a string, diffusion, etc.) therefore a simple exponential decay was postulated:

$$A = A_\infty (1 - e^{-Kt}) \tag{7}$$

where

$A \equiv$ contraction of boron filament expressed in %

$A_\infty \equiv$ asymptotic value of contraction at infinite time

$K \equiv$ rate constant dependent on boundary conditions.

In order to fit the experimental data, K was found to be a product of two rate constants, K_1 and K_2:

$$K_1 = \upsilon e^{-E/kT}$$

$$K_2 = K_0(1 - e^{-\alpha[O_2]}).$$

By substitution, one obtains the equation:

$$A = A_\infty \left\{1 - \exp\left[-tK_0\upsilon e^{-E/kT}\ (1 - e^{-\alpha[O_2]})\right]\right\}. \tag{8}$$

Fitting this equation to the experimental data gave values for E, A_∞, $K_0\upsilon$, and α shown below:

$A_\infty = -1.89\%$

$K_0\upsilon = 37.87\ \text{sec}^{-1}$

$\alpha = 40$

$E = 0.97$ eV

It must be emphasized that equation (8) is an empirical relationship constructed to fit the experimental data presented, and that the physical meaning of the values found is as yet not completely known. An interesting point to

note was that the effective activation energy, determined by the present work, (0.97 eV) was near the midpoint of the range in activation energies determined by DiCarlo[33] in similar experiments.

Several examples of the spectacular interfacial void formations, that were observed in the annealed boron filament, are shown in Figures 25, 26 and 27. Figures 25 and 26 are micrographs (SEM) of B/W filament that had been annealed at different temperatures in air. Complete separation of the boron sheath from the core was apparent in filament that were annealed at temperatures of 1100°C and above. This allowed the core to buckle along the length of the filament. Core buckling was probably due to the high axial compressive stresses present in the core, causing it to increase its length when the constraint of the boron sheath was removed by separation through void formation. Consider that the voids formed an annular ring around the core. Measurements were made from a number of SEM micrographs of annealed filament cross-sections, and these measurements indicated that the average thickness of the annular rings were: 3.1μm @ 1100°C; 4.5 μm @ 1150°C; and 7.7 μm @ 1200°C. All of these measurements pertain to boron filament annealed in air for 300 seconds (5 minutes). Figure 27 shows a cross-section (27a) and core region (27b) view of a B/C filament that was annealed at 1200°C in air for 5 minutes. Figure 27 seemed to imply that the interfacial void formation was not

dependent upon the core material, but rather a phenomenon of the boron sheath. X-ray diffraction was employed to determine whether any structural changes had taken place in the tungsten boride core, or the boron sheath, during annealing at 1200°C for 5 minutes. Analysis of the x-ray pattern for as-produced and annealled filament revealed them to be identical. Split boron filament were annealed in air at 1200°C for 3 minutes, and then, the tungsten boride core was removed by etching with a 30% hydrogen peroxide (H_2O_2) solution. Voids were observed to have formed at the core - boron sheath interface, and an example of such a filament is shown in Figure 28. Figure 28 is an oblique view of the split filament, and Figure 28b is a view of the core - sheath interface. The voids shown in Figure 28b appeared to have formed axial rows corresponding to die marks on the tungsten substrate, which probably served as preferred nucleation sites for the void formation. This indicated a possible similarity between the interfacial void formation, and the nucleation and growth of the boron deposit and the formation of "proximate voids"[34]. These annealed split filament were thinned from the outside with an ion beam, and examined by transmission electron microscopy. Small voids were observed at the core - boron sheath interface. Two examples of these voids are shown in Figures 29 and 30b. Figure 29 depicts a void that appeared to have been in the early stages of

development. Electron diffraction revealed that small crystals were present at the interface near the center of the void, and the d spacing values determined from the diffraction pattern corresponded to β-rhombohedral boron.[35] Figure 30b shows another void at the core - sheath interface of an annealed boron filament. It was noted that the structural appearance of the void region resembled the "tangerine peel" processes, which are clearly seen on the surface of the voids shown in Figure 26. Electron diffraction of the process shown in Figure 30b revealed that they also contained small crystals of β-rhombohedral boron. The formation of β-boron crystals at the surface of the voids was consistent with earlier observation[36] that amorphous boron crystallized by surface nucleation, rather than nucleation in the bulk. X-ray energy dispersive analyses of the interfacial void regions detected no tungsten in the core - sheath interface region of the boron mantle.

Microstructural Observations - Split as-produced boron filament were thinned on an ion-milling machine for examination in a transmission electron microscope (TEM). Specimens were thinned from the outside and from the inside, in order to observe microstructural features present in the core - sheath interface region and the outer surface region, respectively. Figure 30a is a typical example of a core - sheath interface region. Dark regions of various sizes and

shapes were observed to be imbedded in the otherwise featureless material of the interface region, and electron diffraction revealed the entire region to be "amorphous" boron displaying the typical halo pattern with d values of 4.3, 2.5, 1.7, and 1.4 angstroms. It appeared that the dark islands observed were small regions of more dense boron imbedded in a less dense boron matrix. Figures 31 and 32 are TEM micrographs of the outside surface region of boron filaments. An interesting feature was noted to be present in the outer surface region of more than 50% of the filaments examined. This "rod" structure appeared to be composed of rodes of dense boron with less dense boron between the rods. Also shown in Figures 31 and 32 are large voids that had formed in some, but not all, of the less dense regions surrounding the rods. The size of the voids ranged from approximately 100 Å to 1000 Å. It was presumed that the ion-beam thinning process could have enlarged the voids; however, the mere presence and consistent locations of the voids in the less dense regions indicated the existence of voids in these regions prior to thinning. A typical "rod" diameter was found to be on the order of 2000 Å. The distance which the rods extended into the boron sheath was estimated to be approximately 3 μm. Electron diffraction patterns of the "rod" structure regions revealed no difference in structure between the dense "rods" and the less

dense areas. It was noted that the d values for the outside and inside regions of an as-produced boron filament were the same. The "rod" structure shown in Figures 31 and 32 could possibly have a relationship with the "hillock" feature observed by Wawner.[1] Figure 33 shows regions of the outer surface portions of boron filament in which the "rod" structure was absent. These regions did, however, reveal the presence of small voids, with a typical diamter of approximately 100 Å, which appeared to be randomly distributed throughout the areas examined. Again, electron diffraction patterns of the regions shown in Figure 33 indicated the same "amorphous" structure as shown in Figure 30. These observations suggested that a low concentration of voids existed in the interior portions of the boron sheath; whereas, a high concentration of voids, some quite large, existed in the outer regions of the boron sheath. This was in agreement with the result found by DiCarlo,[37] which showed that the density of the boron sheath increased from the outside to the core interface.

SUMMARY AND CONCLUSIONS

The elongation of boron/carbon filament was studied, and it was determined that increasing the tension on the substrate, by addition of weight, increased the elongation. Different deposition gases were used, (i.e., "depleted" BCl_3 and "plant" BCl_3) and the difference in elongation produced by the use of these gases was found to be insignificant when compared to other factors, such as deposition temperature. Deposition temperature has an interesting effect on the B/C filament. The elongation of the boron during deposition was sufficient to cause fracture of the carbon core. If the deposition temperature is high enough, then creep can occur in the carbon substrate, allowing it to elongate with the boron sheath, thus minimizing fracture of the core. At lower deposition temperatures, a phenomenon called "light bulbing" resulted. The "light bulbing" was due to electrical discontinuities arising from core fracture. Rapid growth of boron, which was generally crystalline, resulted at these points. The amount of "light bulbing" influenced the elongation, since the fracture of the substrate reduced the constraint to the elongation. This "light bulbing" effect can be reduced, but not eliminated, by coating the carbon substrate with a thin layer ($\simeq$1 μm) of pyrolytic graphite (PG). An analysis of boron elongation could not easily be made because of this "light bulbing" phenomenon. It was found that the elongation

was linear with the final radius squared (R^2) for the early stages of deposition, and non-linear for the later stages of deposition. An important result was found by using a carbon substrate. It was found that a negative elongation of approximately 1% occurred when crystalline boron was deposited.

Boron deposition experiments were also performed on different diameter tungsten substrates (i.e., 5.1 μm, 13 μm, 17.8 μm, 33 μm, 38 μm and 43 μm). The elongation was found to be as great as 16.6% for the smallest tungsten wire substrate and below 2% for the largest tungsten substrate. This difference could be attributed to the presence of unreacted tungsten in the larger cores of the filament, which would restrain the elongation due to diffusion and reaction of boron with the tungsten substrate. The elongation was studied as a function of deposition temperature, using a 13 μm diameter tungsten substrate. It was found that during the early stages of deposition the elongation was dominated by core development into WB_4 and W_2B_5, and that during the later stages of deposition, the elongation was due to the elongation of the boron sheath. An empirical relationship was found that gave a satisfactory fit to all the B/W elongation data:

$$\Lambda = \Lambda_0 \left(\frac{R - r_c}{R + r_c} \right)^n$$

where

$R \equiv$ final radius of the filament

$r_c \equiv$ radius of the core

A_0 and n were fitting parameters.

The deposition temperature variation experiments allowed evaluation of A_0 and n, which yielded two effective activation energies, 0.33eV and 0.27eV. These energies were quite low for atomic migration phenomena, and no definite explanation of these energies can be offered at this time.

As-produced boron filaments were also used as substrate. It was found that the elongation phenomenon was a continuous function of the filament radius, whether the deposition was interrupted and performed in steps, or was continuous.

Elongation of boron filaments was studied in relation to small amounts of doping of the deposition gas mixture using tungsten hexaflouride (WF_6), silicon tetrachloride ($SiCl_4$) and methane (CH_4). No definite effect on elongation was found by the addition of small amounts of W via WF_6 or Si via $SiCl_4$. However, at higher concentrations the co-deposition of boron and tungsten onto a tungsten substrate produced a filament composed of WB_2. Incorporation of carbon in the boron deposit via CH_4 did have a definite effect on the elongation (i.e., the higher the carbon content, the lower the elongation). X-ray diffraction analysis of each set of filaments that had a different carbon content revealed that the decrease in elongation was accompanied by an increase in crystallinity of the boron-carbon deposit.

A model was presented in an effort to explain the origin of the boron elongation phenomenon. The assumption was made that the boron atoms were deposited individually and in a random distribution. After being covered by fresh deposit, boron atoms underwent a transformation into icosahedron that resulted in an expansion that proceeded as:

$$\left[1 + (f - 1)\ (1 - e^{-Kt})\right]$$

where

t ≡ the time at which the boron layer was deposited

f ≡ expansion factor

K ≡ rate constant

An expansion resulting from the boridization of the tungsten core was also taken into account. The correct behavior was seen from the elongation curves generated by the model, and the residual stresses given by the transformation model were in fair agreement with those determined experimentally.

Boron filaments were annealed in various atmospheres and contractions of the filaments were observed. It was found that the contraction was dependent upon the concentration of oxygen in the annealing atmosphere and annealing temperature. A simple exponential decay to equilibrium from a non-equilibrium state was postulated:

$$A = A_{\infty}\ (1 - e^{-Kt})$$

where

A_{∞} ≡ asymptotic value of contraction (%)

$K \equiv$ rate constant

$t \equiv$ annealing time.

The rate constant K was found to be the product of two rate constants: $K = K_1 K_2$

where

$$K_1 = \upsilon e^{-E/kT}$$

and

$$K_2 = K_0 \ (1 - e^{-\alpha[O_2]})$$

Fitting this equation to the experimental data gave the values:

$A_\infty = -1.893$

$K_0 \upsilon = 37.87 \ sec^{-1}$

$\alpha = 40$

$E = 0.97eV$

The effective activation energy E = 0.97eV was found to lie near the midpoint of the energy range obtained by DiCarlo[33] in similar experiments. Large interfacial void formations were observed in the annealed boron filament. These were most probably due to the diffusion of boron atoms outward, and subsequent "vacancy" diffusion inward, which condensed at the core - sheath interface. Small crystals of ß-rhombohedral boron were found to have formed in "tangerine peel" processes visible at the inside surface of the voids.

Appropriately thinned split boron filament were examined in a transmission electron microscope. A "rod" structure was found to exist near the outer surface in most

of the filament examined. Voids of varying size were observed to be present near the outside surface in all the filament studied. The inside surface (core - sheath interface) of as-produced filament revealed no significant concentration of voids. Electron diffraction disclosed that the outer regions, whether the "rod" structure was observed or not, and the inner regions had the same "amorphous" structure.

It was concluded that the elongation was fundamentally dependent upon: (1) deposition temperature; (2) substrate type and size; and (3) quantity of boron deposited. The origin of the B/W filament elongation could be explained by an expansion in the boron sheath due to a transformation of boron atoms into random icosahedra and expansion of the tungsten substrate due to boridization. Annealing boron filament in an environment that allows boron atoms to be removed from the surface at a sufficiently high temperature resulted in recovery of the elongated boron sheath from its initial elongation. This was caused by interfacial void formation. The density gradient found experimentally by DiCarlo[33] was most probably the result of a void concentration difference between the outer and inner surface of the boron sheath.

REFERENCES

1. F. Wawner, "Boron Filaments", Modern Composite Materials, ed. by Broutman and Krock, Addison and Wesley, 1967, p. 244.

2. D. R. Behrendt, "Axial Residual Stresses in Boron Fibers", NASA TM-73894; 2nd International Conference on Composite Materials, Toronto, Canada, April 16-20, 1978.

3. H. Rogers, "Research on Improved High Modulus, High Strength Filaments and Composites Thereof", AFML-TDR-65-319, September 1965.

4. R. Witucki, "High Modulus High Strength Filaments and Composites", Technical Report AFML-TR-66-187, May 1967.

5. K. Faughnan, "Longitudinal Residual Stresses in Boron Filaments", 20th Annual Tech. Cong., Reinforced Plastics/Composites Institute, 1974.

6. G. Layden, "Fracture Behavior of Boron Filaments", J. Mat. Science 8, 1581 (1973).

7. H. DeBolt, V. Krukonis, J. McKee, R. Prescott, and F. Wawner, "Development and Demonstration of a Low Cost Boron Filament Formation Process", AMFL-TR-72-271, 1972.

8. C. Talley, J. Appl. Phys., 30, 114, 1959.

9. H. DeBolt, et al., "Lower Cost High Strength Boron Filament", AFML-TR-70-287, June 1971.

10. R. Diefendorf and R. Mehalso, "Vapor Deposition of High Strength-High Modulus Boron on a Mono-Filament Substrate", 3rd Intl. Conf. on Chemical Vapor Deposition, Salt Lake City, Utah, April 1972, p. 552.

11. F. Tavadze, "Low Temperature Internal Friction Peaks in Boron Fibers", Mekhanzmy Vnutrennego Treniya v poluprovodnikurykh I. Met. Mat., AKH 9103, 1972, p. 4.

12. G. Gunyaev, et al., "Effect of Temperature on the Mechanical Properties of Boron Fibers", Mekhanika Polimerou, No. 2, March-April, 1971, p. 329.

13. F. Tavadze and G. Tsagaireshuili, "Crystalline Boron", Soviet Science Review, No. 1972, p. 357.

14. J. DiCarlo, NASA Technical Memorandum, NASA TM X-71907 May 1976 and NASA TM X-71710 March 1977.

15. Mehalso, R. M., "Chemical Vapor Deposition of Boron on a Carbon Monofilament Substrate - A Study of Residual Stresses and Deposition Kinetics", Ph.D. Thesis, Rensselaer Polytechnic Institute, Troy, N. Y., Nov. 1973.

16. F. Wawner, Private Communication.

17. Diefendorf, R. J., Williams, R., "Elongation - Residual Stress Studies of C.V.D. Boron Filament on a Tungsten Substrate", Technical Report, NASA-Lewis Research Center, June, 1976.

18. Witucki, R. M., "High Modulus, High Strength Filaments and Composites", Technical Report AFML-TR-66-187, May 1967.

19. Woods, H. P., Wawner, F. E., Fox, B. G., "Tungsten Diboride: Preparation and Structure", Science 151:75, 1966.

20. Ploog, et al., J. Less-Common Metals 29:161, 1972.

21. Thompson, R., Progress in Boron Chemistry, New York: Permagon Press, 1970, p. 173.

22. Lipsitt, H. A., Otte, H. M., "On the Interpretation of Electron Diffraction Patterns from 'Amorphous' Boron", Phys. Status Solidi. 13:439, 1966.

23. Gorski, L., "A New Orthorhombic Polymorph of Boron", Phys. Status Solidi. 3:316, 1963.

24. Decker, B. F., Kasper, J. S., "Crystal Structure of a Simple Rhombohedral Form of Boron," Acta Cryst. 12:503, 1959.

25. Hoard, J. L., Hughes, R. E., Sands, D. E., "The Structure of Tetragonal Boron," J. Am. Chem. Soc. 80:4507, 1958.

26. Hoard, J. L., "Structure and Polymorphism in Elemental Boron," Borax to Boranes, Advan. Chem. Series No. 32, (American Chemical Society, Washington, D. C., 1961) p. 42.

27. Hughes, R. E., et al, "The Structure of β-Rhombohedral Boron," J. Am. Chem. Soc. 85:361, 1963.

28. Katada, K., "Electron Diffraction Study of Evaporated Boron Fibers," Japanese J. Appl. Phys. 5:581, 1966.

29. Blackburn, L. D., Herzog, J. A., Meyerer, W. J., et al, "MAMS Internal Research on Metal Matrix Composites," MAM-TM-66-3, 1966.

30. Thebault, J., Pailler, R., Bontemps-Moley, G., Bourdeau, M., Naslain, R., "Chemical Compatibility in Boron Fiber -Titanium Composite Materials", J. Less-Common Metals, 47:221, 1976.

31. Street, K. N., Tai, N. T., Hearn, D., "Thermomechanical Behavior of Boron Fibers in Titanium Matrix Composites," J. Less-Common Metals 47:215, 1976.

32. Snide, J. A., "Compatibility of Vapor Deposited B, SiC, and TiB_2 Filaments with Several Titanium Matrices," AFML-TR-67-354, 1968.

33. DiCarlo, J. A., "Mechanisms of Boron Fiber Strengthening by Thermal Treatment," NASA Technical Memorandum 79077.

34. Vega-Boggio, J., Vingsbo, O., Carlsson, J., "The Initial Stages of Growth and the Origin of Proximate Voids in Boron Fibers," J. Mat. Sci. 12:1750, 1977.

35. Hoard, J. L., Newkirk, A. E., "An Analysis of Polymorphism in Boron Based on X-ray Diffraction Results," J. Am. Chem. Soc. 82:70, 1959.

36. Gillespie, J. S., "Crystallization of Massive Amorphous Boron," J. Am. Chem. Soc. 88:2423, 1966.

37. DiCarlo, J. A., Second International Conference on Composite Materials, American Institute of Mechanical Engineers, New York, 1978, pp. 520-538.

TABLE 1

Values of Fitting Parameters A_0 and n in the Equation; $A = A_0\left(\frac{R - r_c}{R + r_c}\right)^n$, by Least Squares Fit to Experimental Data of Deposition Temperature-Dependence Set of Runs.*

Temperature	n	A_0
900°C	2.50	18.93
1000°C	1.96	15.52
1100°C	1.60	12.54
1200°C	1.29	11.14

*r_c = 6.5 μm

TABLE 2

Values of Fitting Parameters A_0 and n in the Equation;

$$A = A_0 \left(\frac{R - r_c}{R + r_c} \right)^n$$, by Least Squares Fit to Core Size Variation Set of Runs.*

r_c	n	A_0
2.6 μm	2.43	22.33
9.1 μm	0.98	5.54
16.9 μm	1.96	5.92
19.5 μm	2.20	6.67
22.1 μm	2.17	6.11

*T = 1200°C

TABLE 3

X-ray Diffraction Analysis of Tungsten Doped Boron Filament Produced With a BCl_3:WF_6 Flow Rate Ratio of 1:1.

Intensity	2θ	d	Compound	hkl
VW	28.84	3.0961	WB_2	001
S	34.25	2.6180	WB_2	100
VS	45.28	2.0026	WB_2	101
W	61.42	1.5095	WB_2	110
W	69.0	1.3610	WB_2	111
VW	79.71	1.2029	WB_2	201

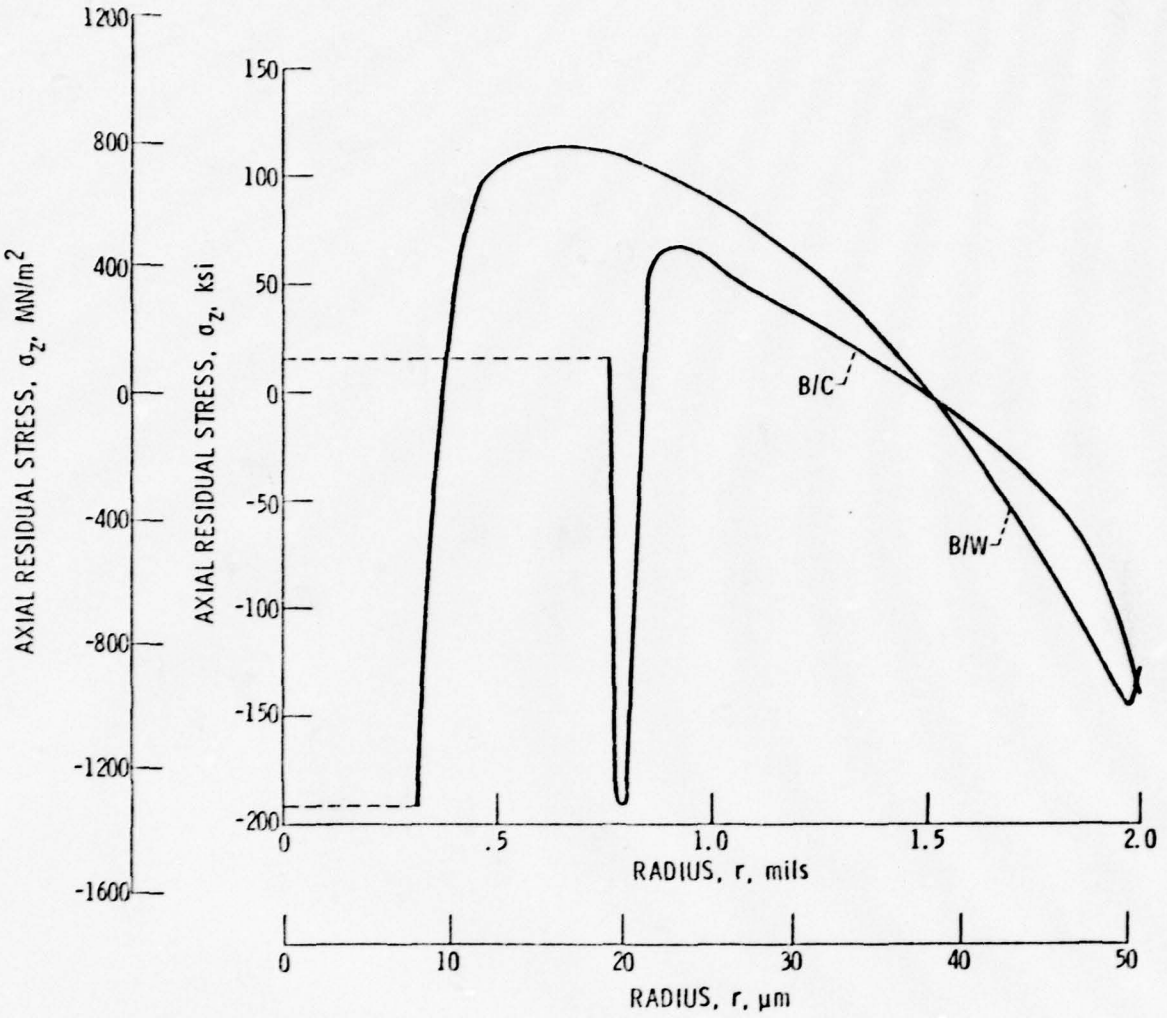

Axial Residual Stress vs. Radius of 102 μm B/W and B/C Filament. From Behrendt

Figure 1

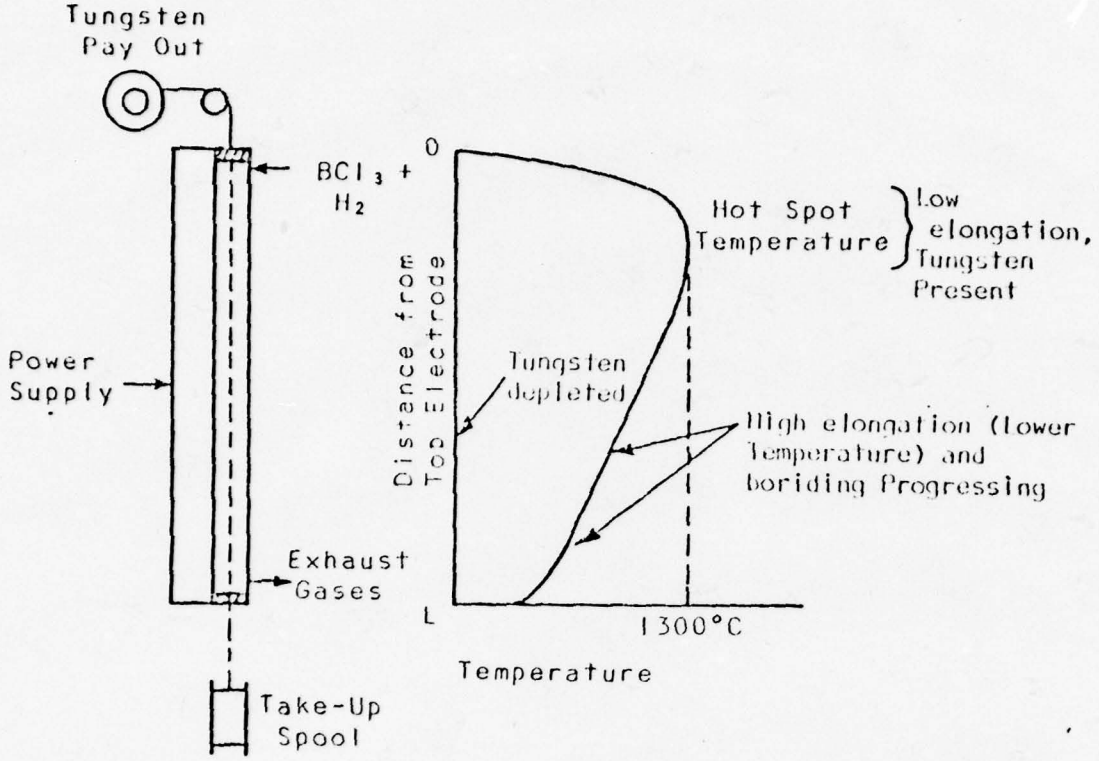

Figure 2

Temperature Profile Within Production Reactor

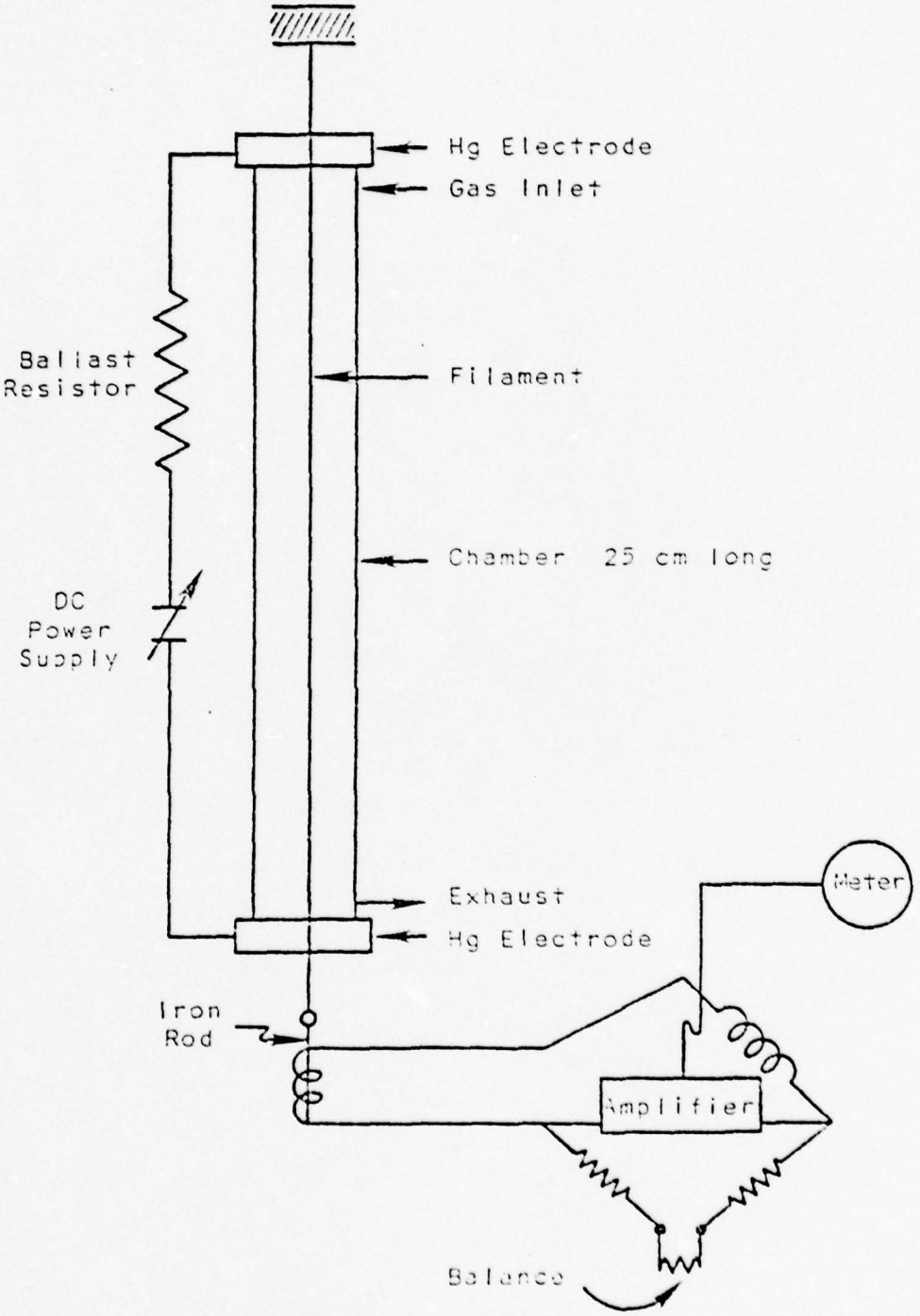

Schematic of Apparatus for Static Elongation Measurements

Figure 3

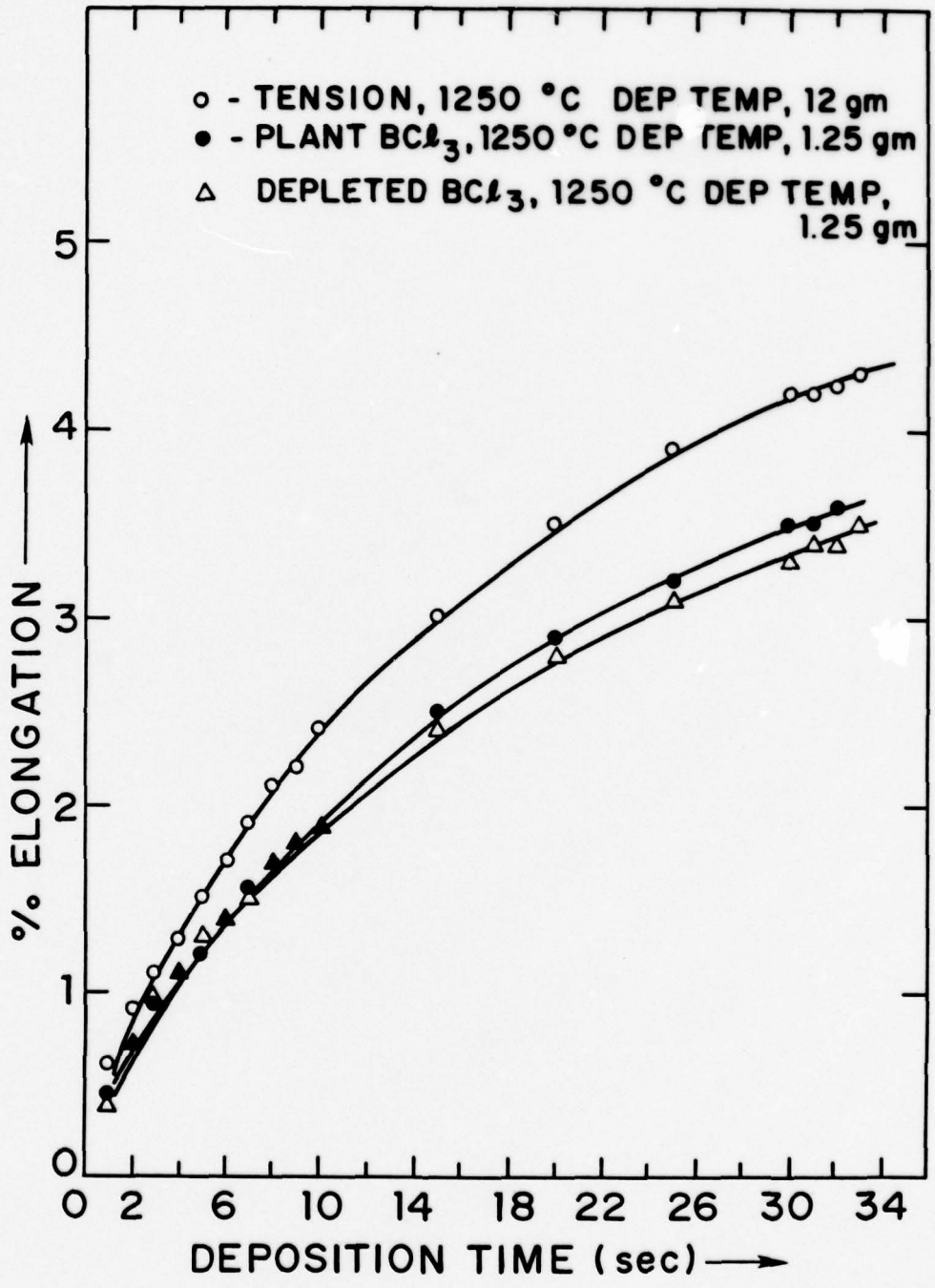

Elongation vs. Deposition Time for B/C Filament

Figure 4

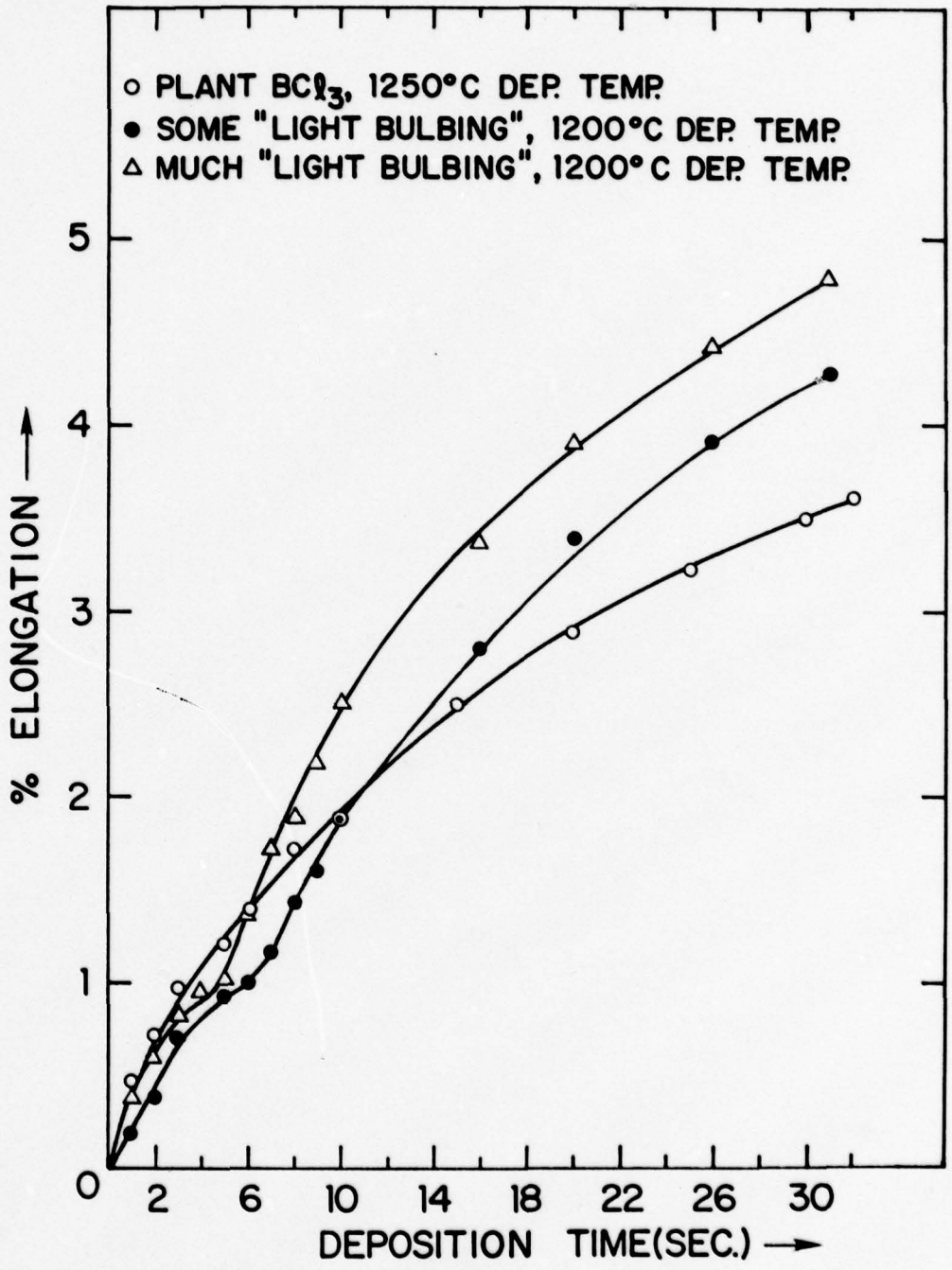

Elongation vs. Deposition Time for B/C Filament.

Figure 5

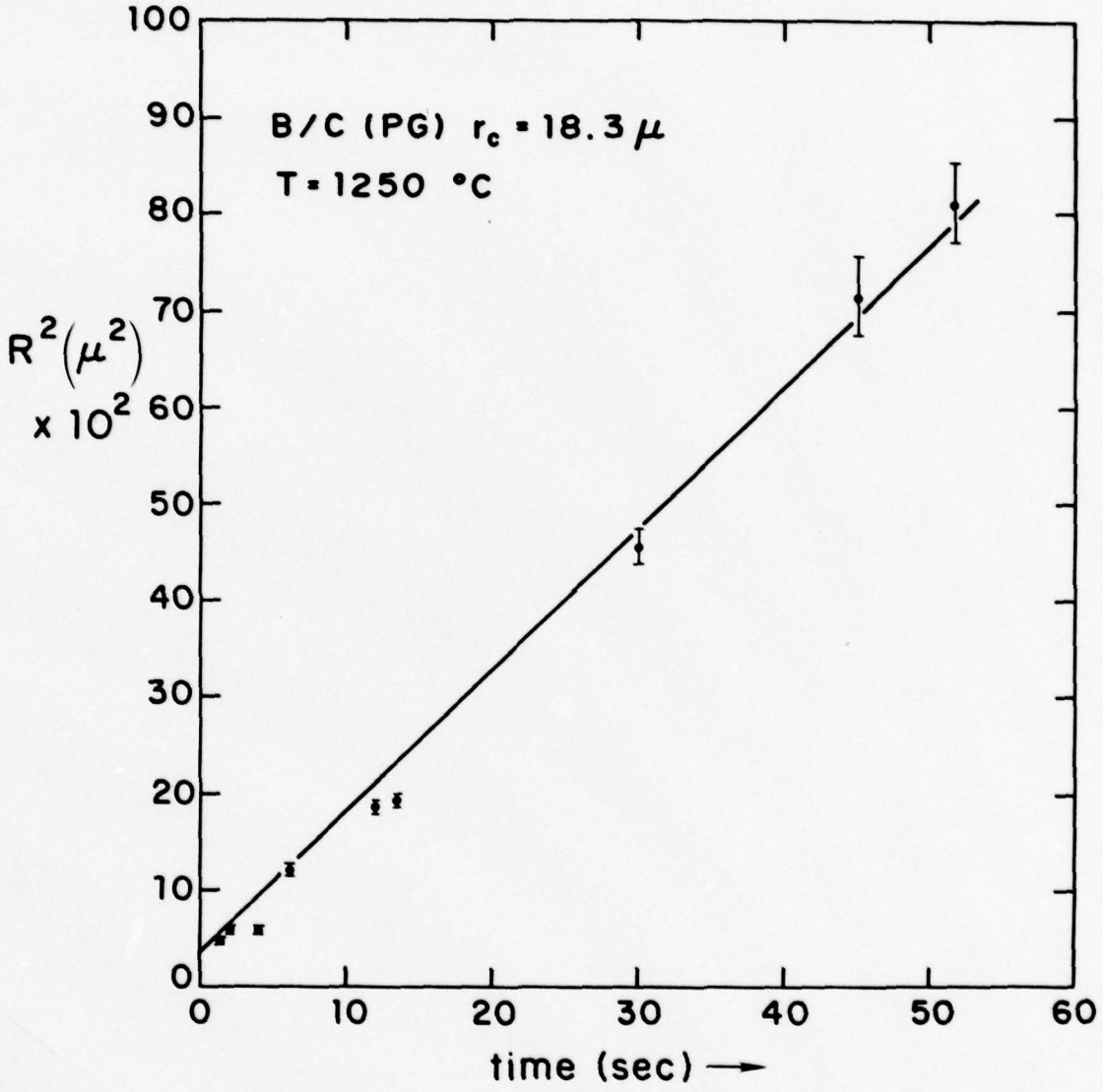

Radius Squared vs. Deposition Time for B/C Filament

Figure 6

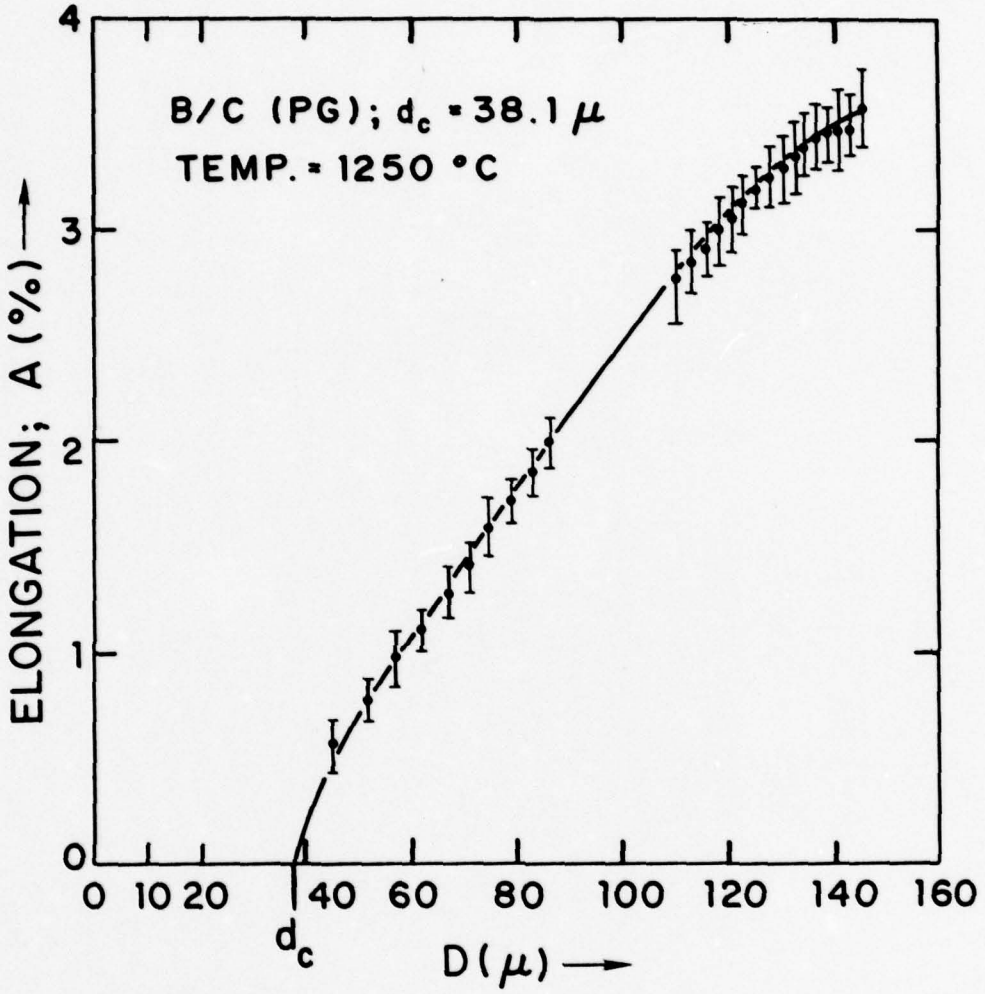

Elongation vs. Diameter of B/C Filament

Figure 7

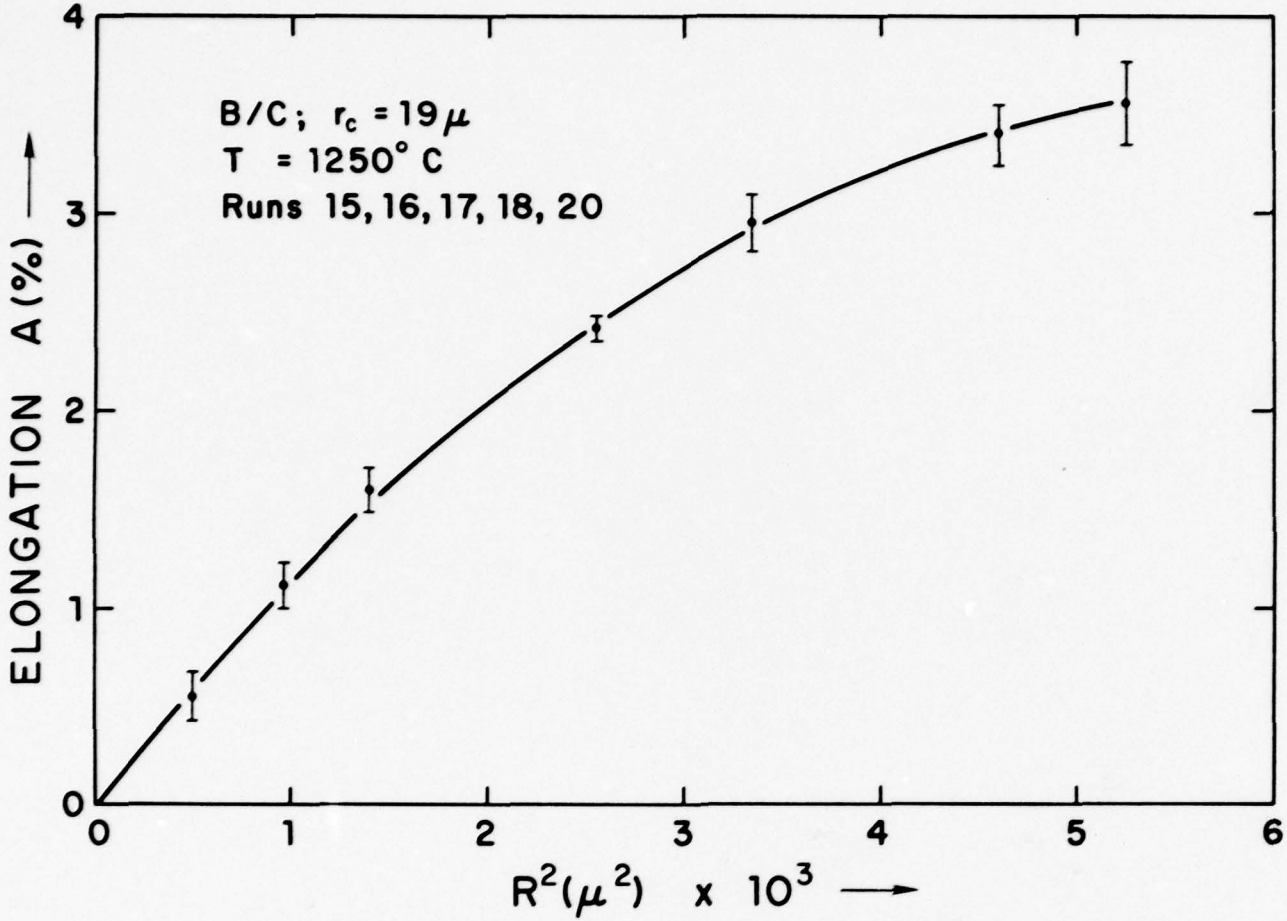

Elongation vs. Radius Squared of B/C Filament

Figure 8

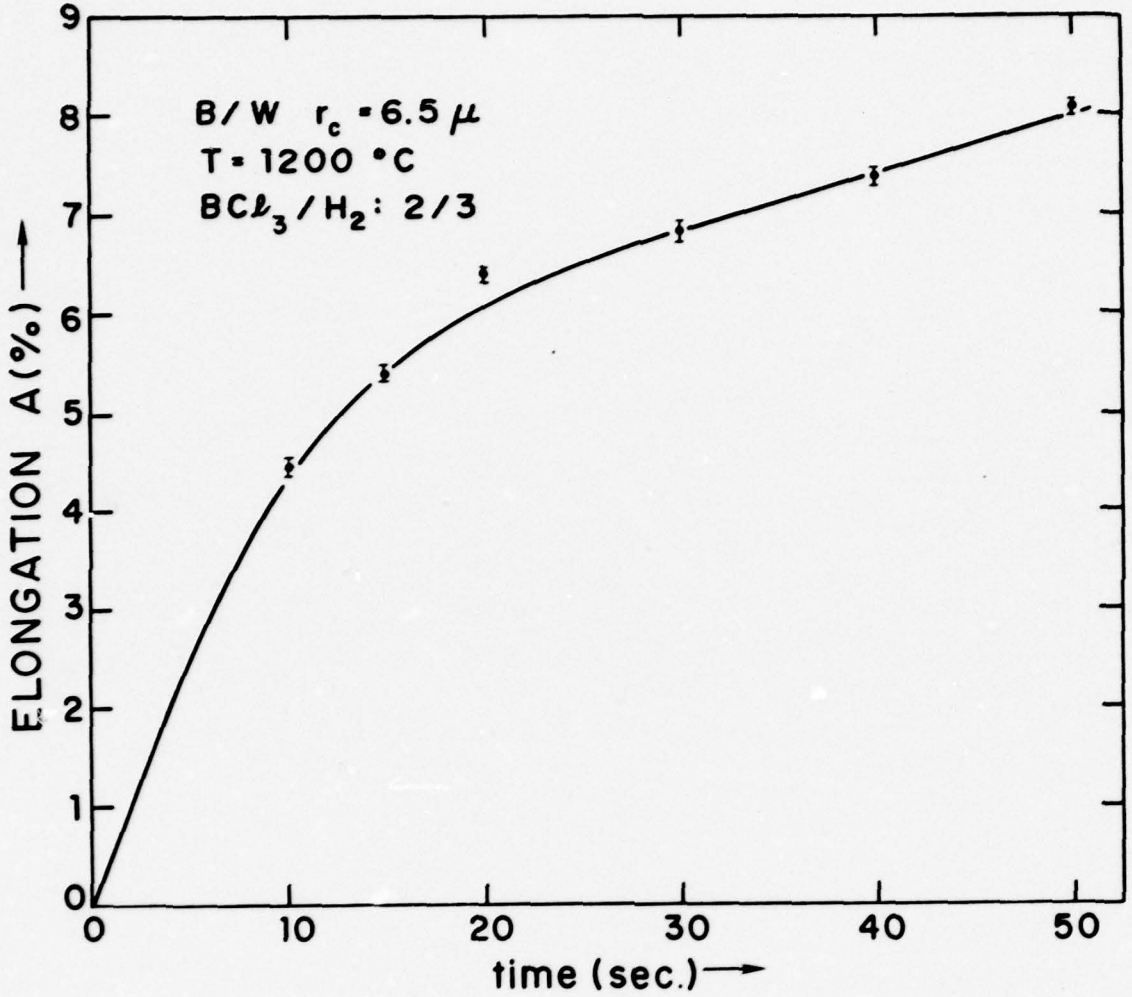

Elongation vs. Deposition Time for B/W Filament

Figure 9

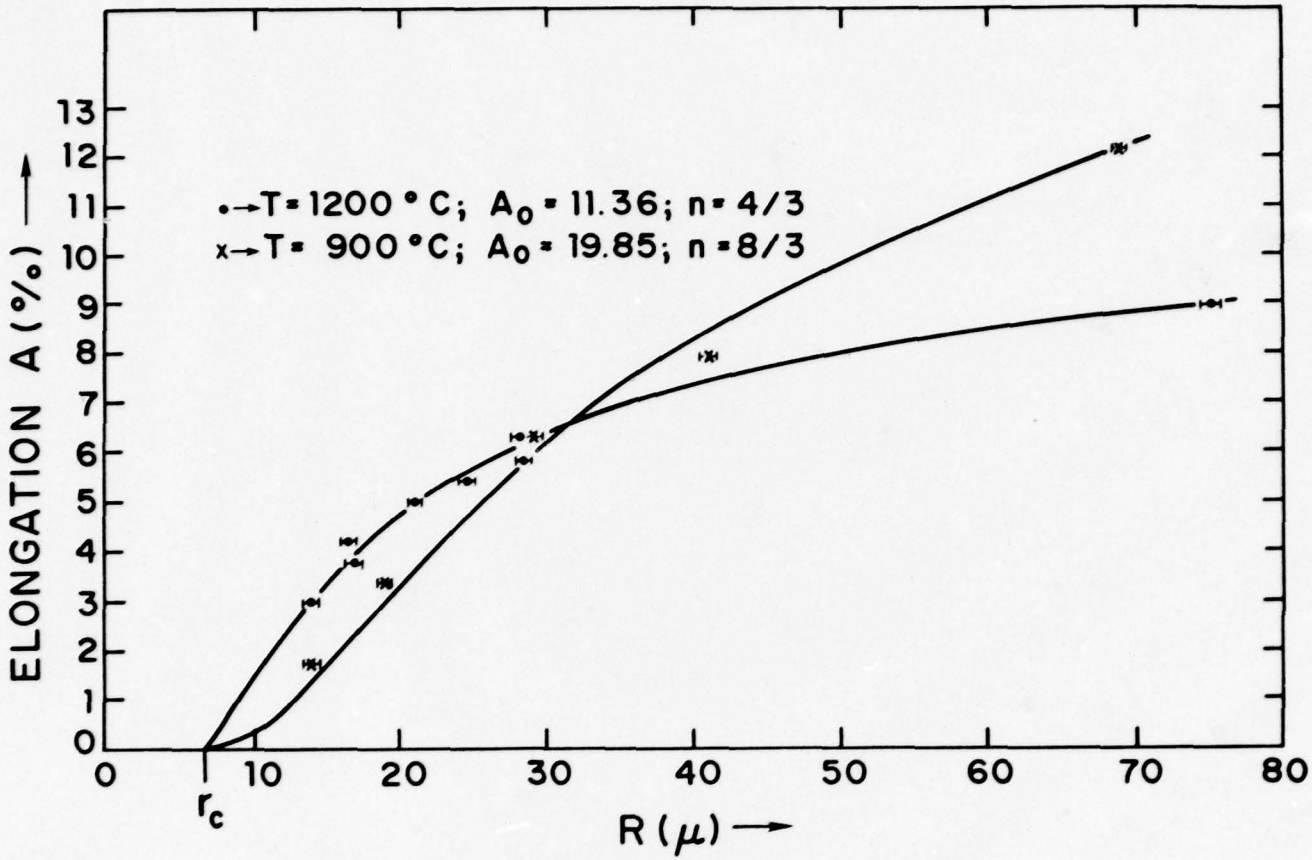

Elongation vs. Radius of B/W Filament
at Different Deposition Temperatures
Figure 10

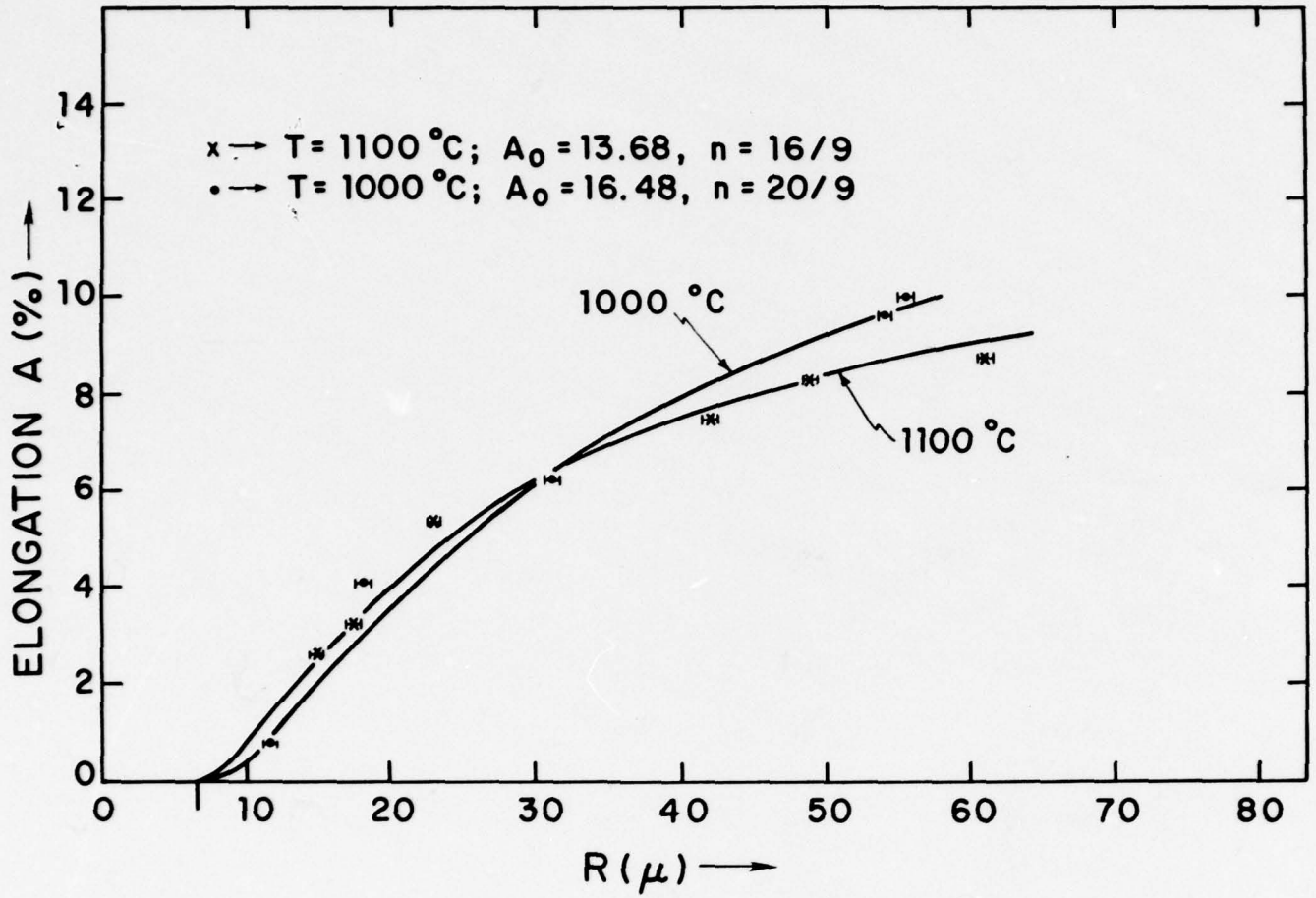

Elongation vs. Radius of B/W Filament
at Different Deposition Temperatures

Figure 11

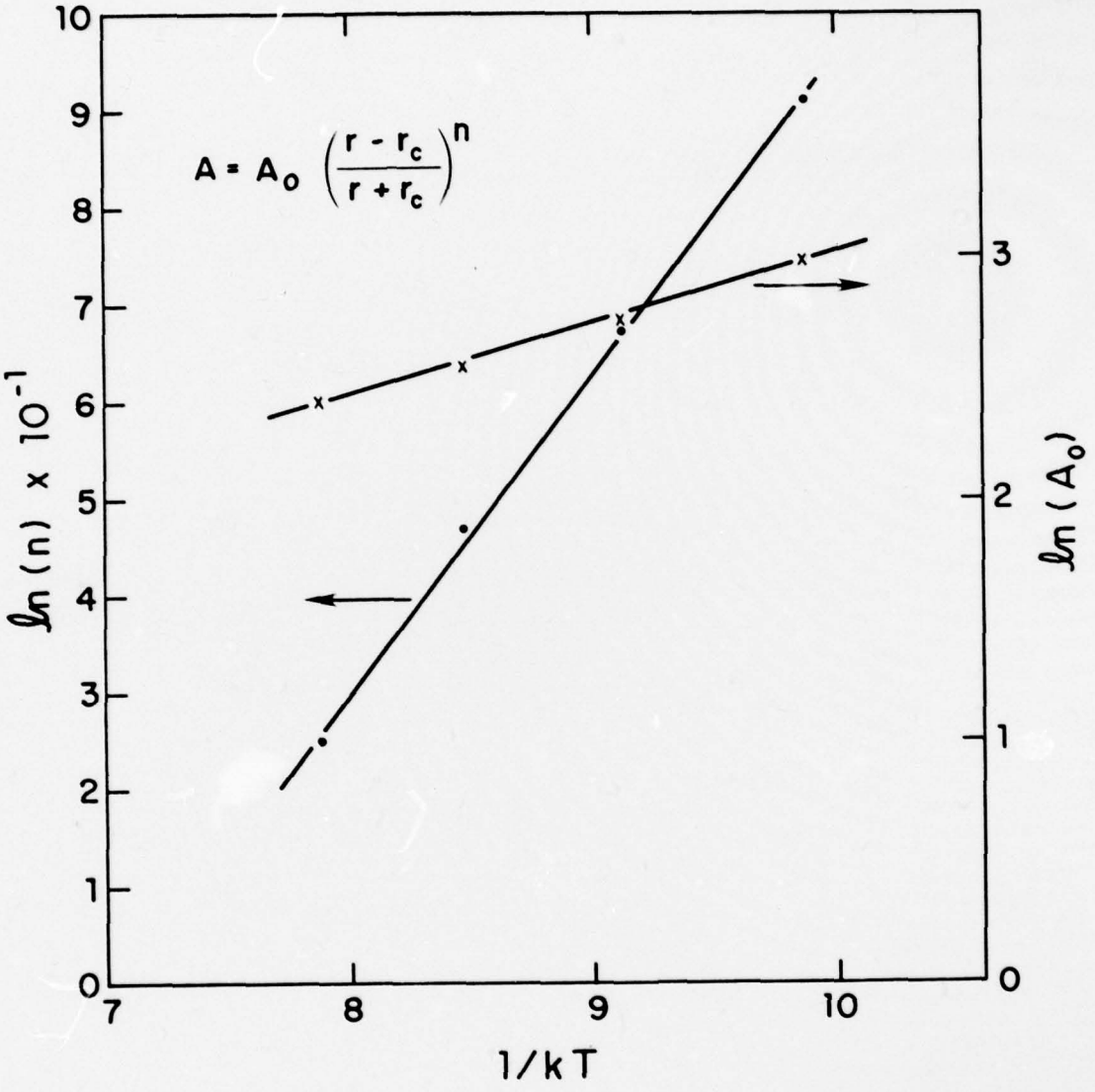

Arrhenius Plot of Fitting Parameters A_0 and n

Figure 12

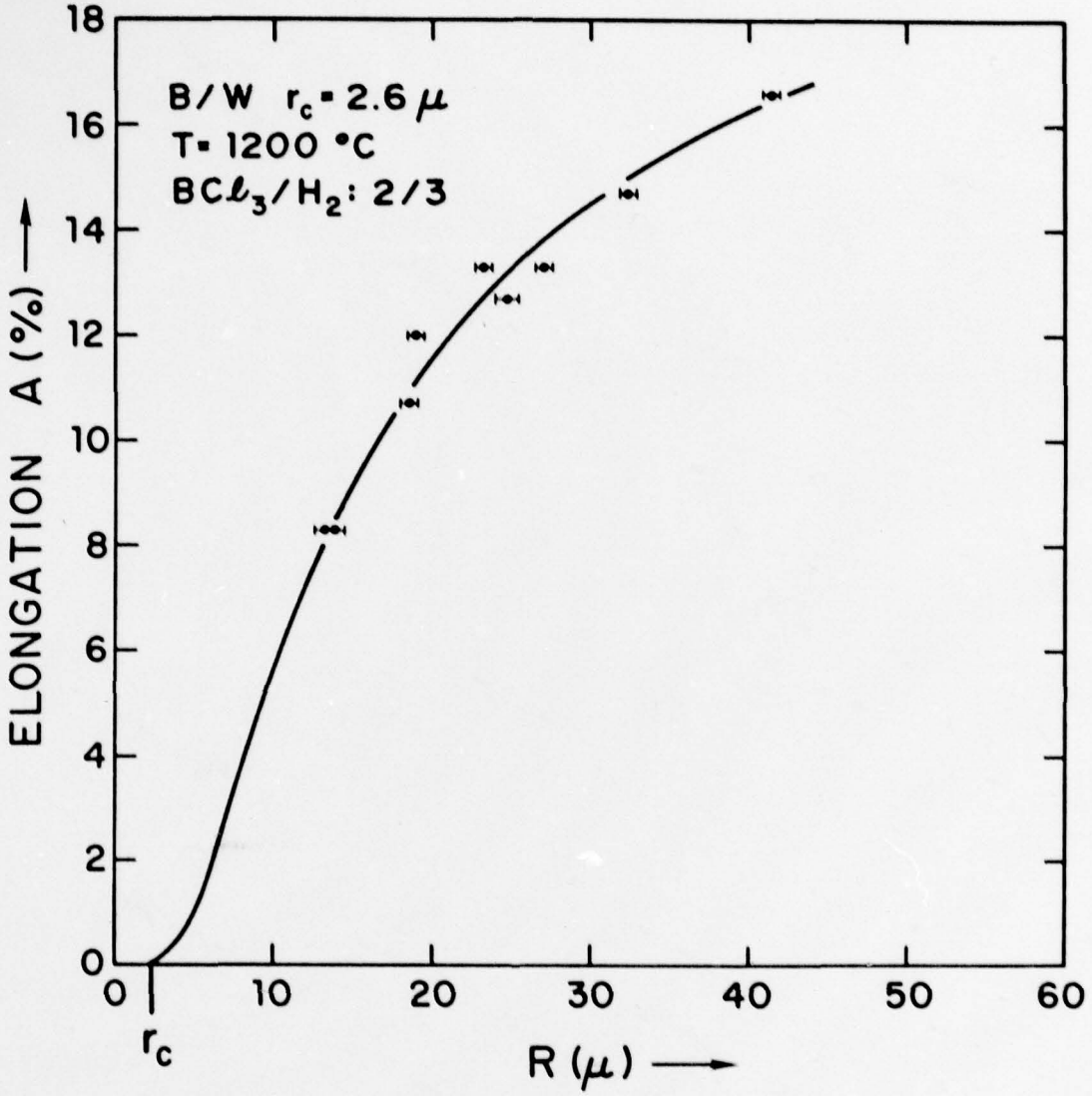

Elongation vs. Radius of B/W Filament with 2.6 μm Radius Tungsten Substrate

Figure 13

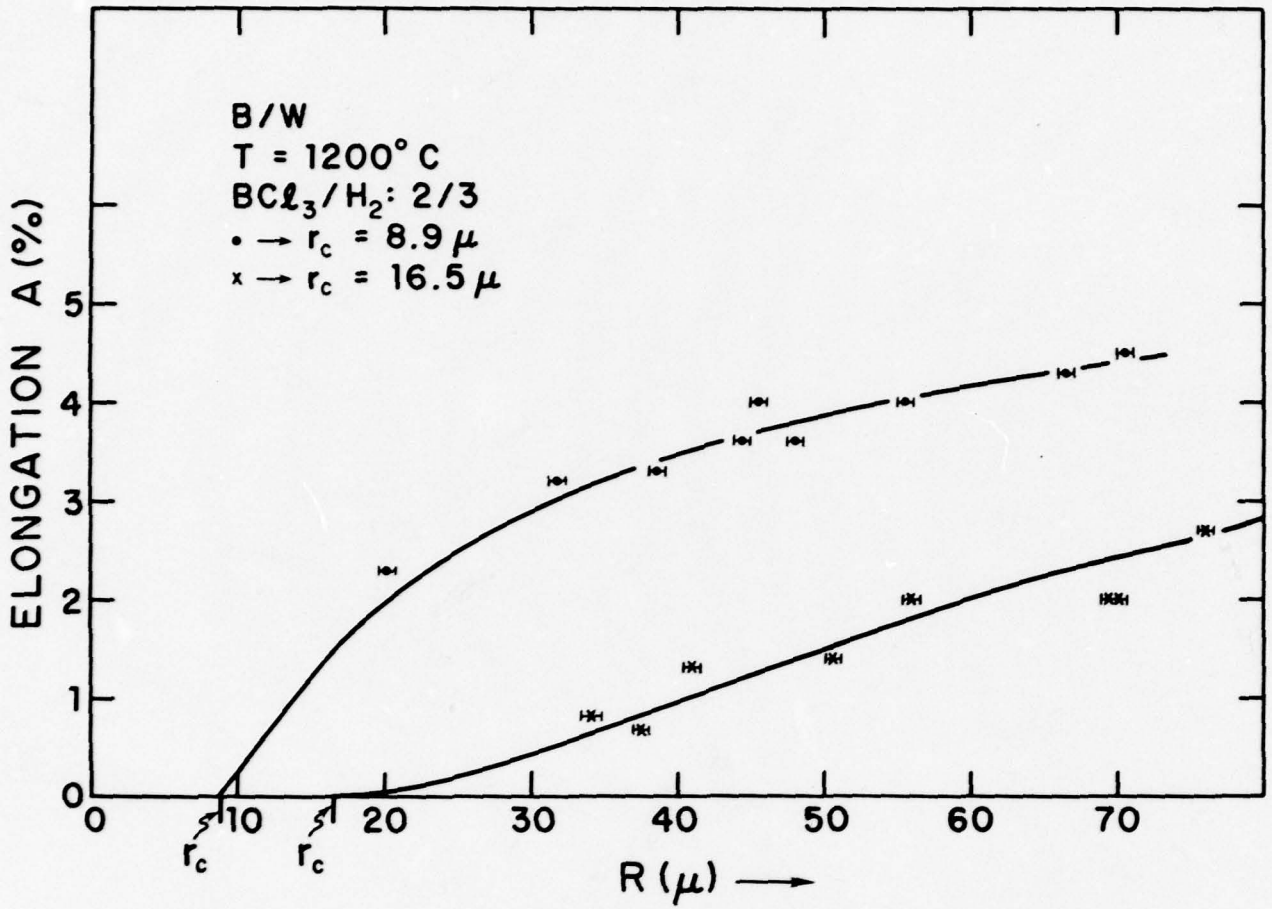

Elongation vs. Radius of B/W Filament
with Different Radius Tungsten Substrates

Figure 14

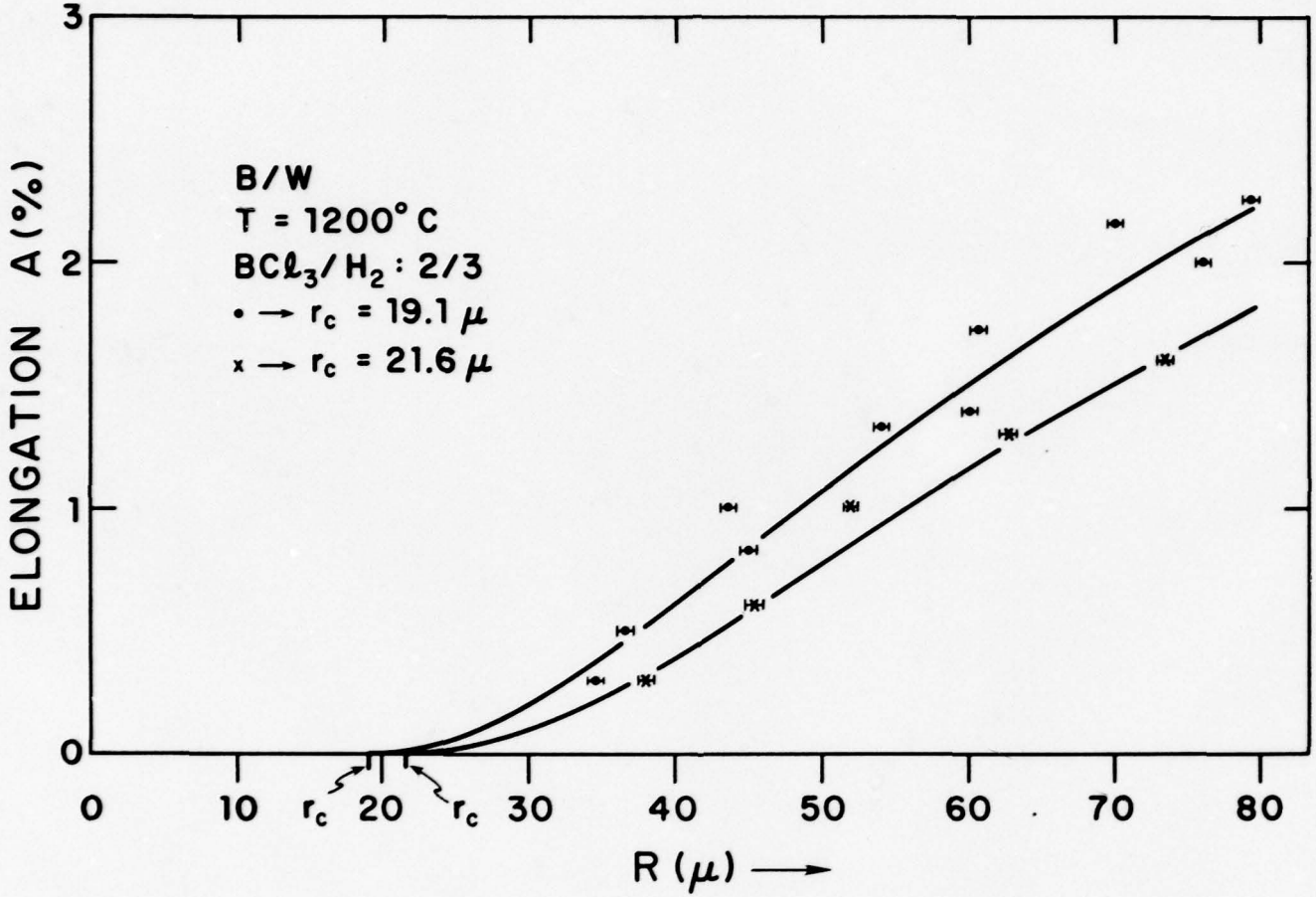

Elongation vs. Radius of B/W Filament
with Different Radius Tungsten Substrates

Figure 15

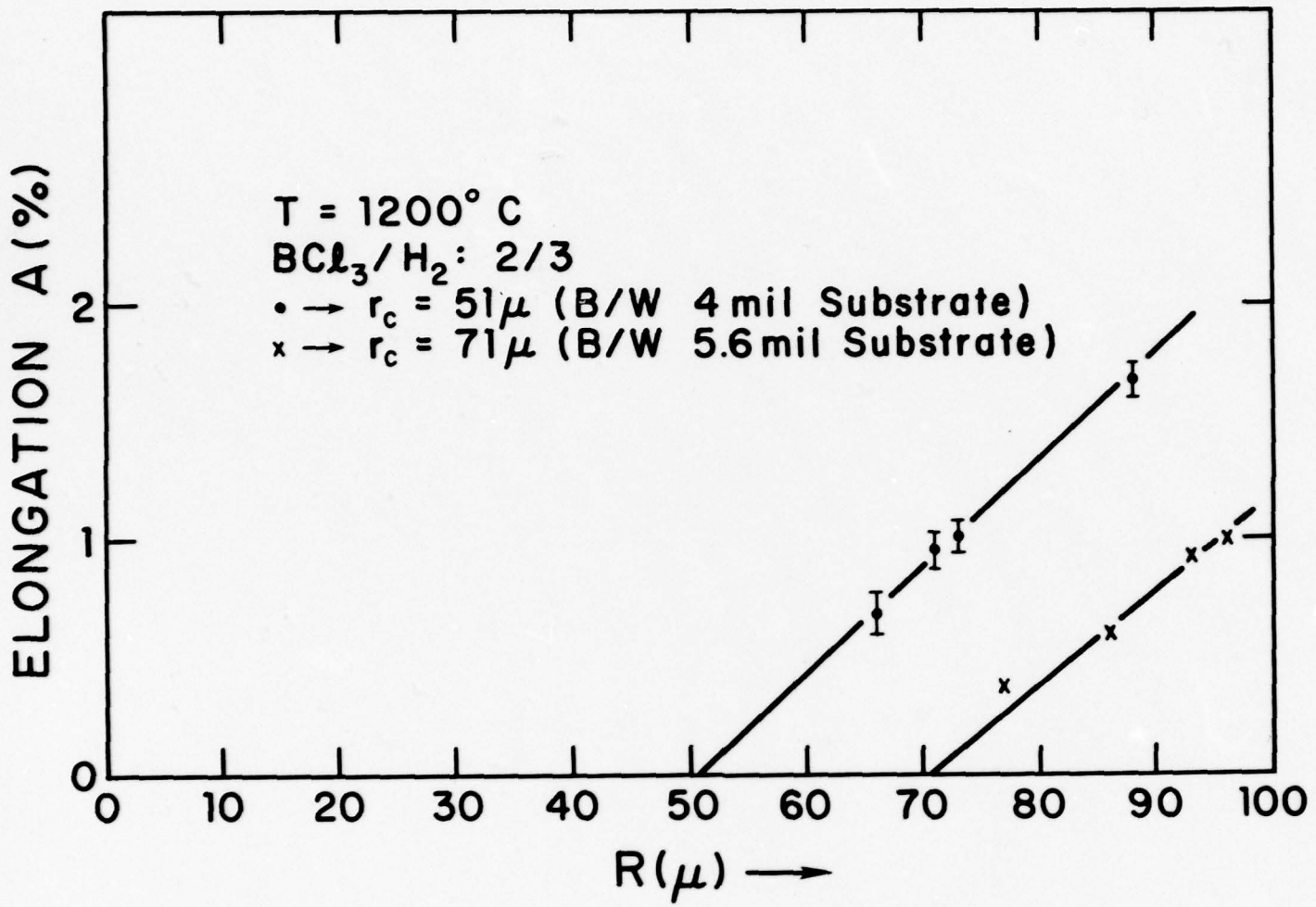

Elongation vs. Radius of B/B Filament with Different Radius Boron Filament Substrates
Figure 16

(a) Cross-section of a tungsten diboride (WB_2) filament.

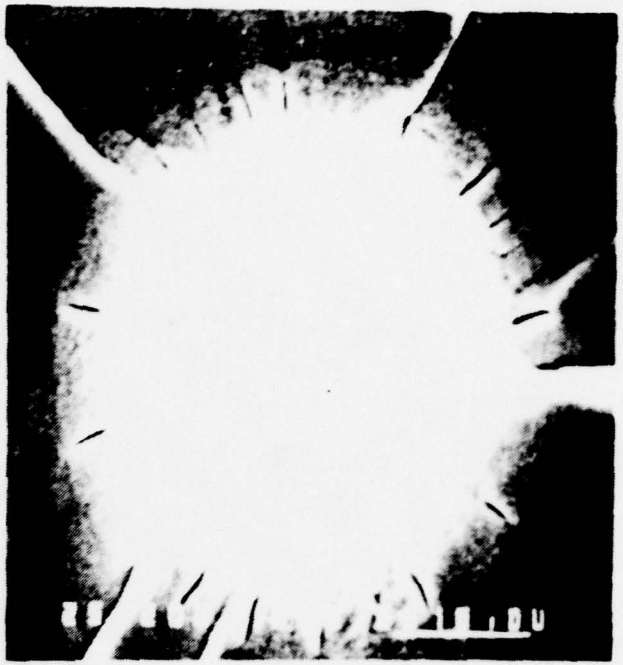

(b) Core region of tungsten diboride (WB_2) filament.

Figure 17

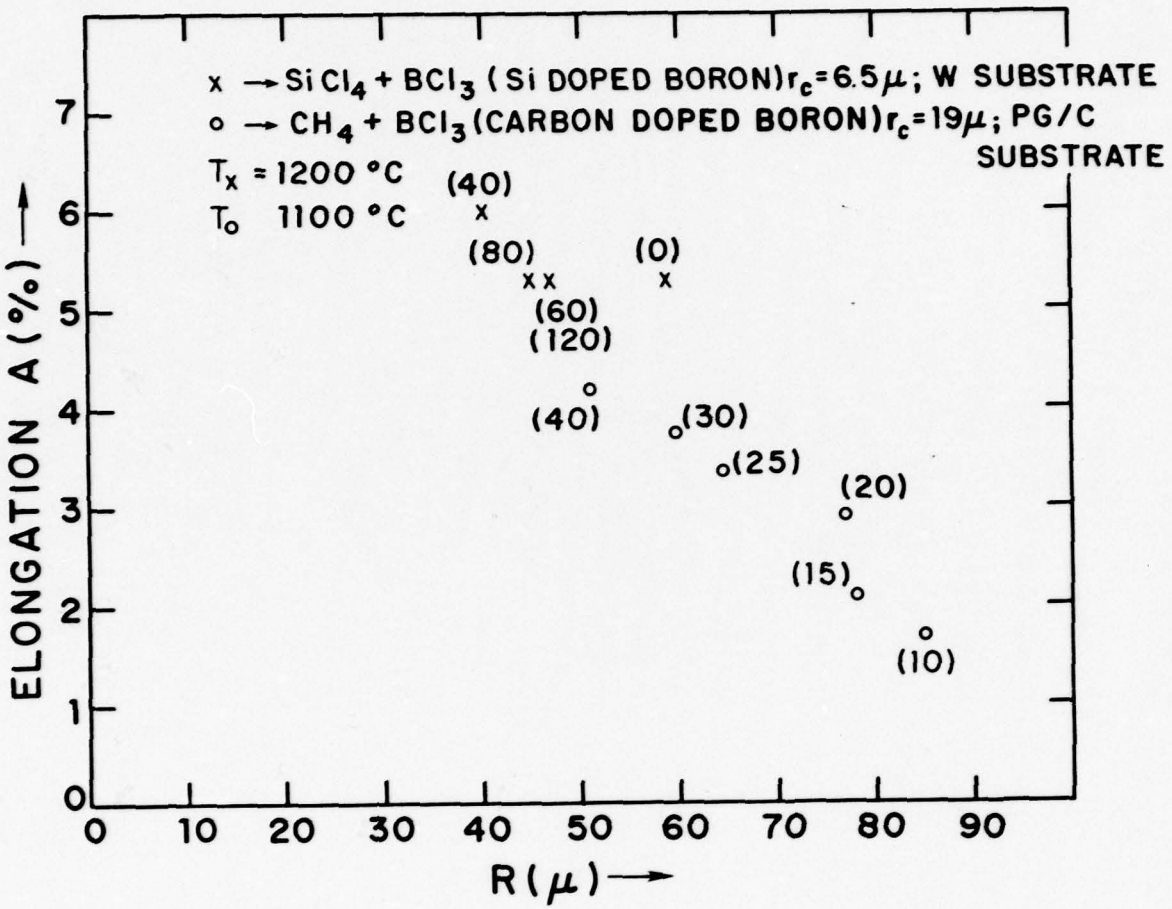

Elongation vs. Radius of Doped Boron Filament

Figure 18

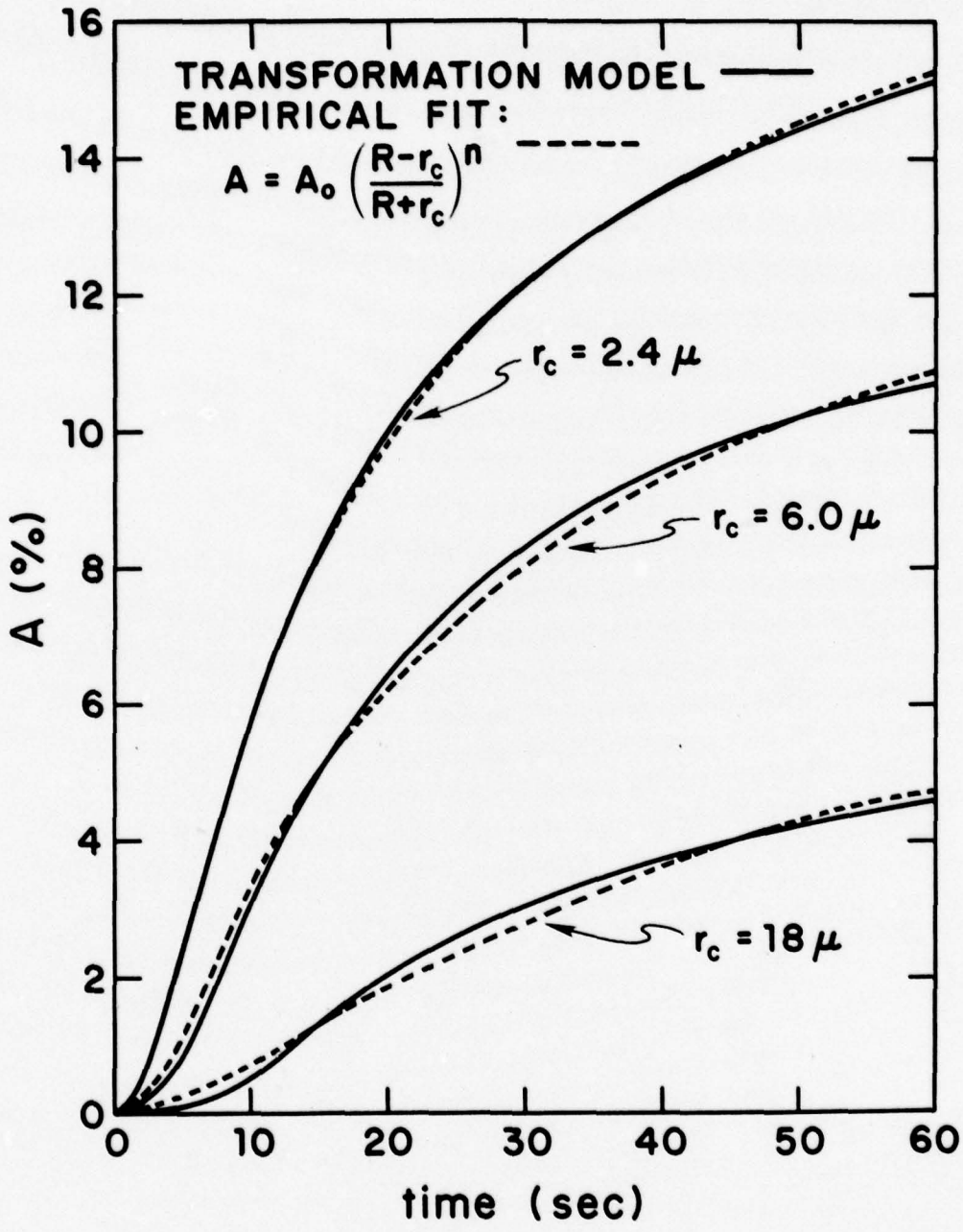

Elongation vs. Deposition Time of
Transformation Model and Empirical Fit

Figure 19

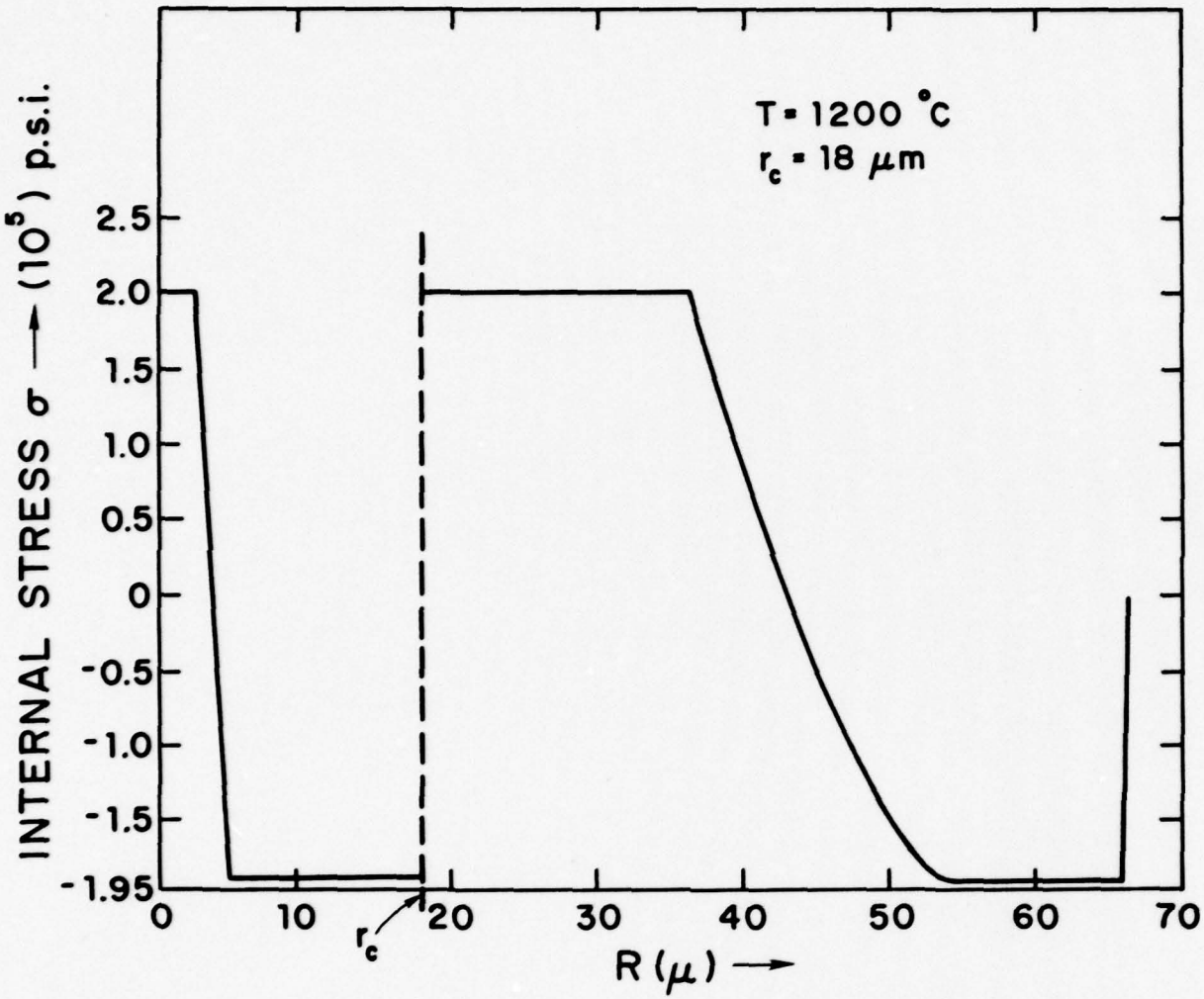

Figure 20

Axial Residual Stress vs. Radius of B/W Filament
as Generated by Transformation Model

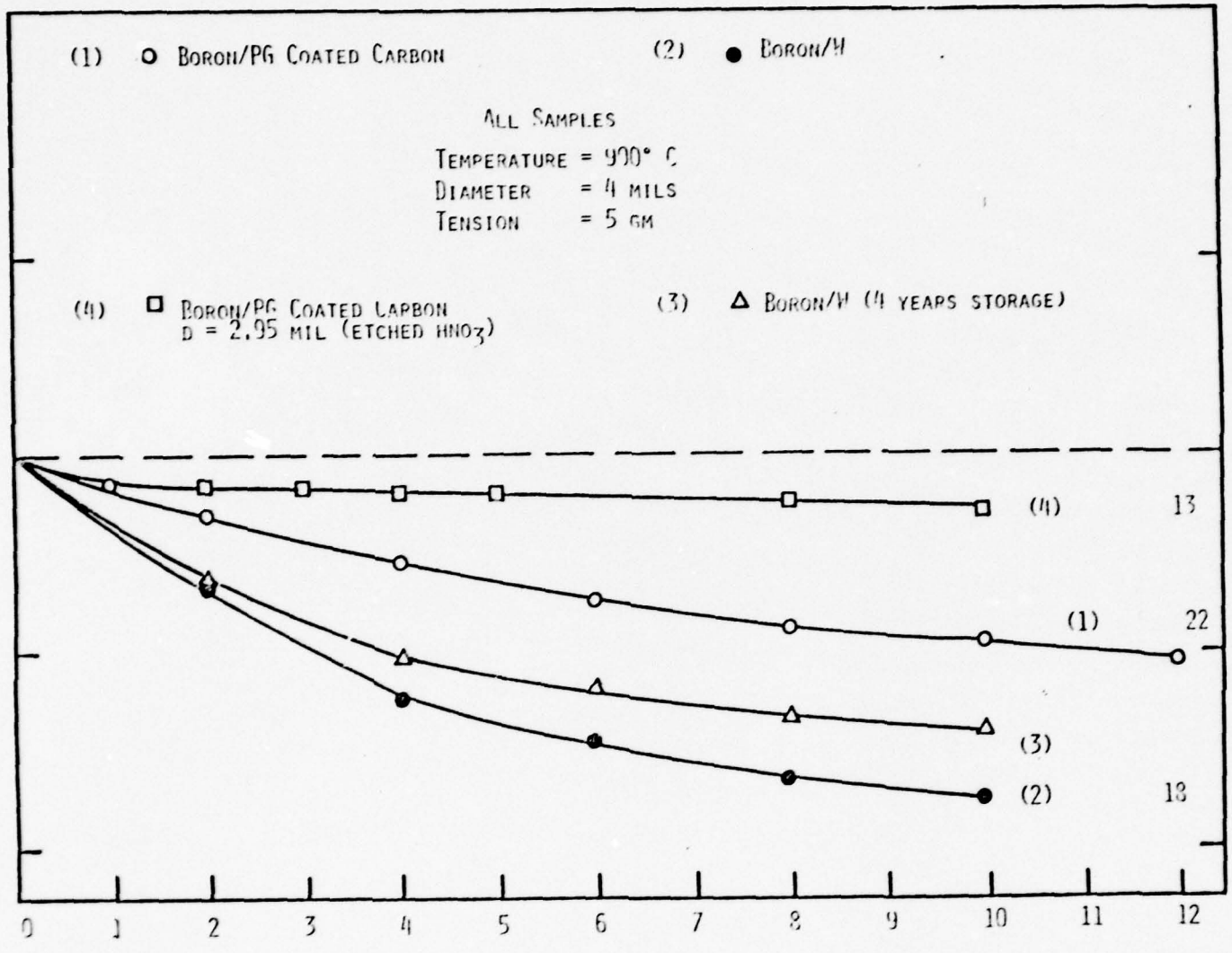

Figure 21 Effect of Heat Treating Boron Filament

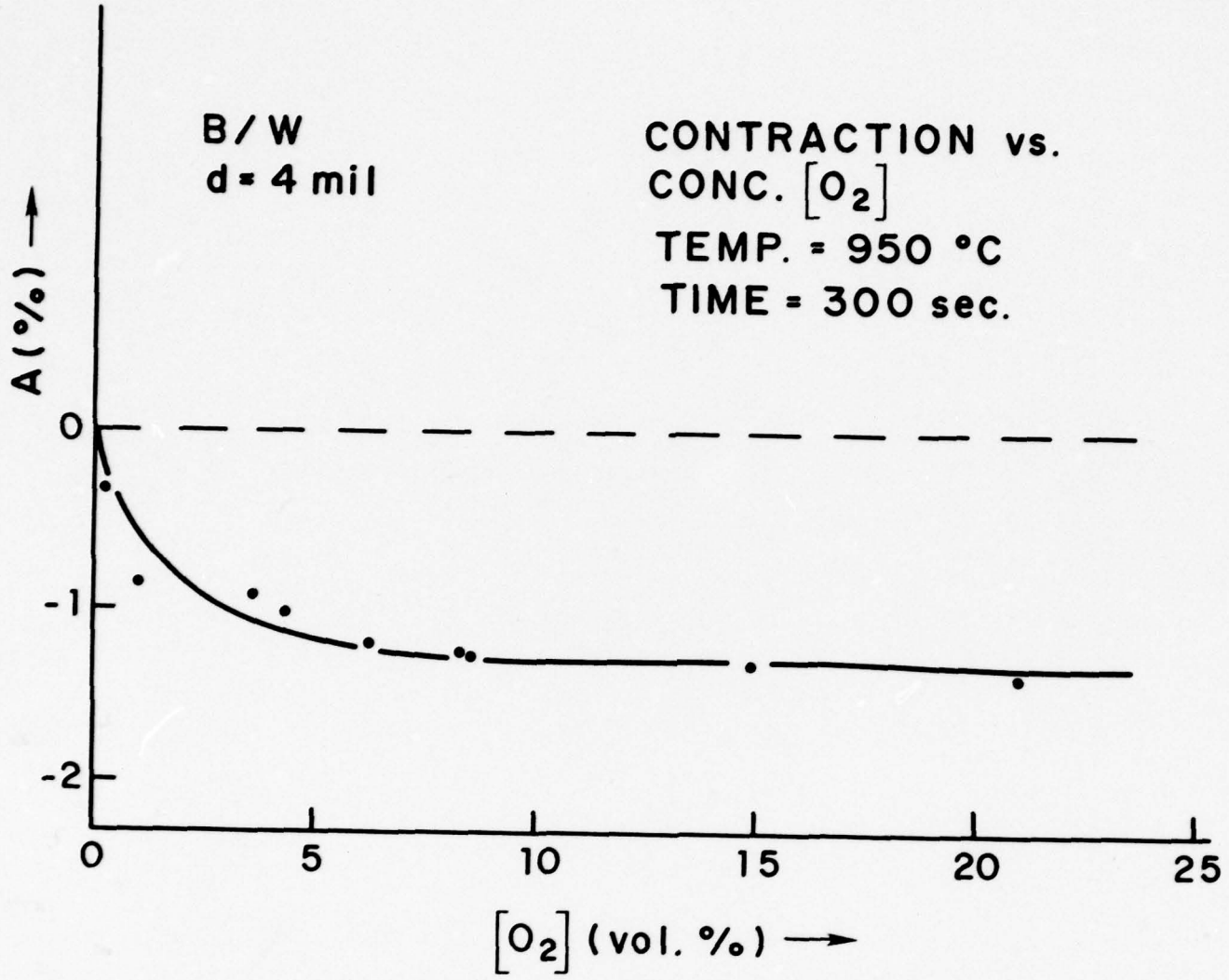

Figure 22

Elongation vs. Concentration of Oxygen
in Annealing Atmosphere for B/W Filament

(a) Surface of B/W filament annealed at 1200°C for 5 minutes.

(b) Core region of B/W filament annealed at 950°C for 5 minutes.

Figure 23

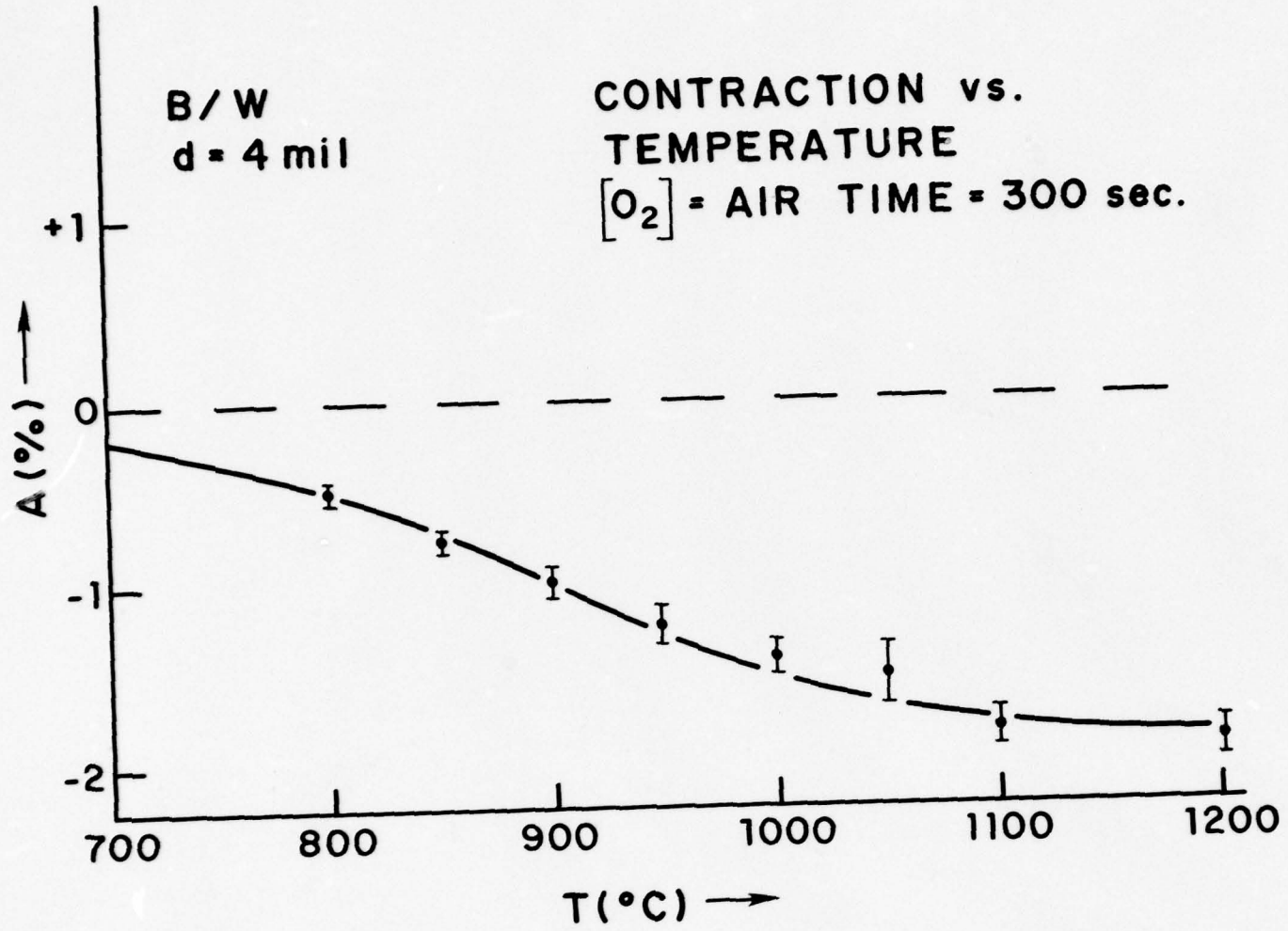

Elongation vs. Annealing Temperature for B/W Filament

Figure 24

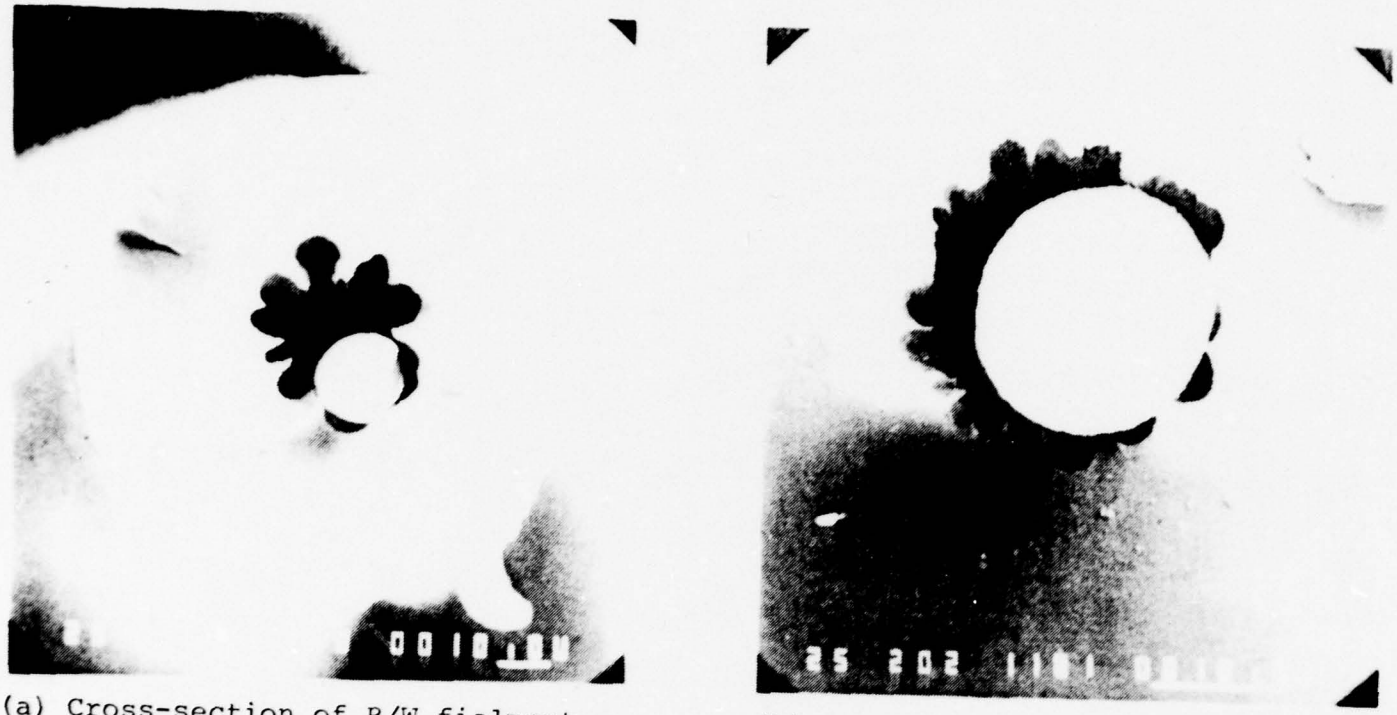

(a) Cross-section of B/W fialment annealed at 1200°C for 5 minutes.

(b) Core region of B/W filament annealed at 1100°C for 5 minutes.

Figure 25

(a) Core region of B/W filament annealed at 1150°C for 5 minutes.

(b) Core region of B/W filament annealed at 1200°C for 5 minutes.

Figure 26

(a) Cross-section of boron on PG coated carbon filament annealed at 1200 C^{o} for 5 min.

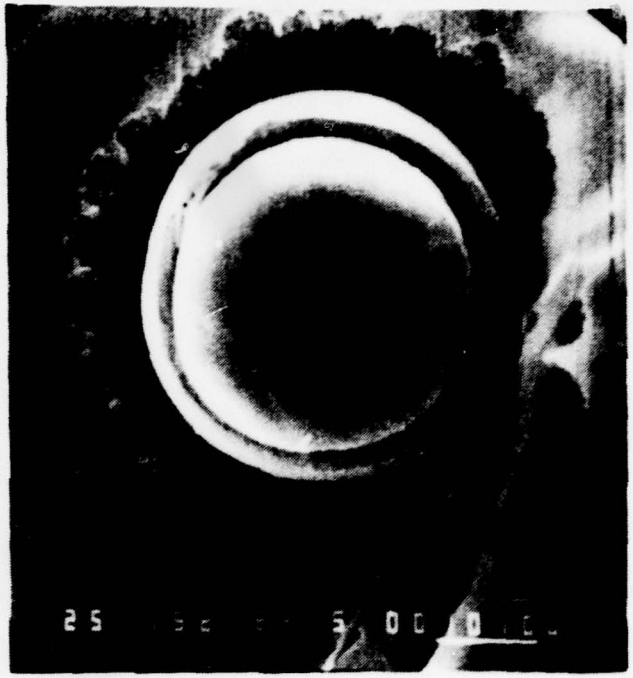

(b) Same as (a); close-up of core region.

Figure 27

(a) Oblique view of split B/W filament annealed at 1200°C for 3 minutes (core removed).

(b) Same as (a); core-boron sheath interface.

Figure 28

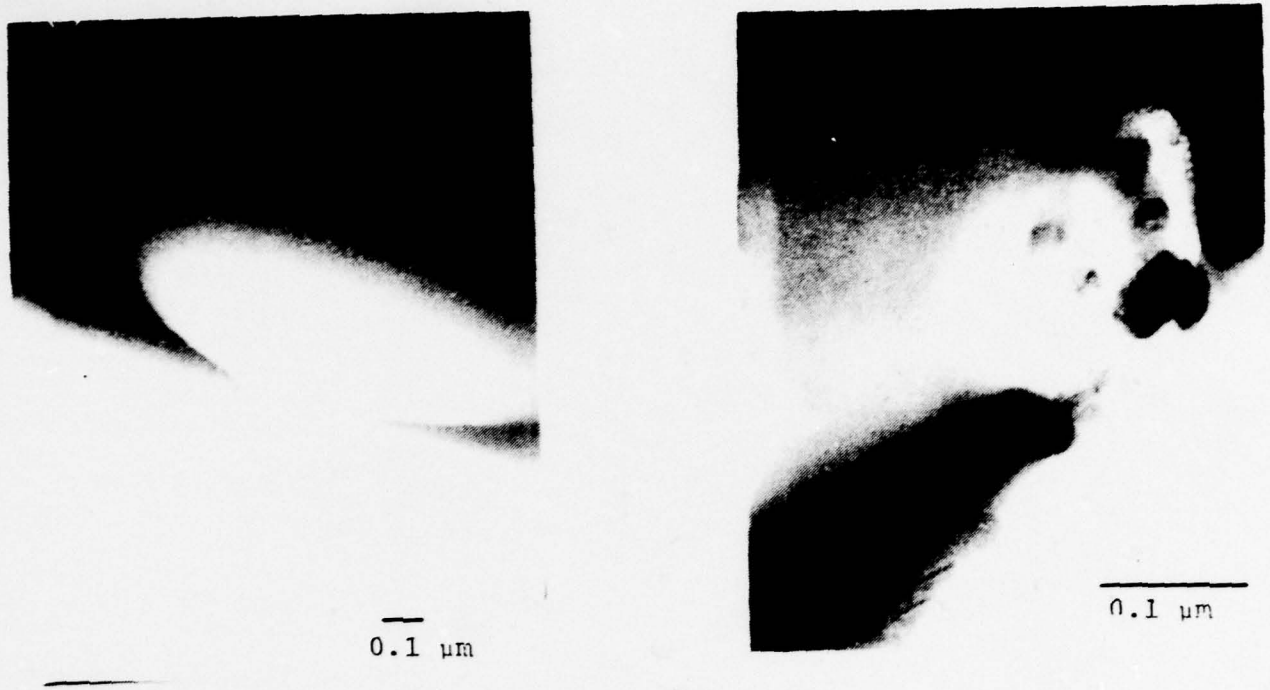

Core-sheath interface region of boron filament annealed in air at 1200°C for 3 minutes.

Figure 29

(a) Core-sheath interface region of as-produced boron filament.

(b) Core-sheath interface region of boron filament annealed in air at 1200°C for 3 minutes.

Figure 30

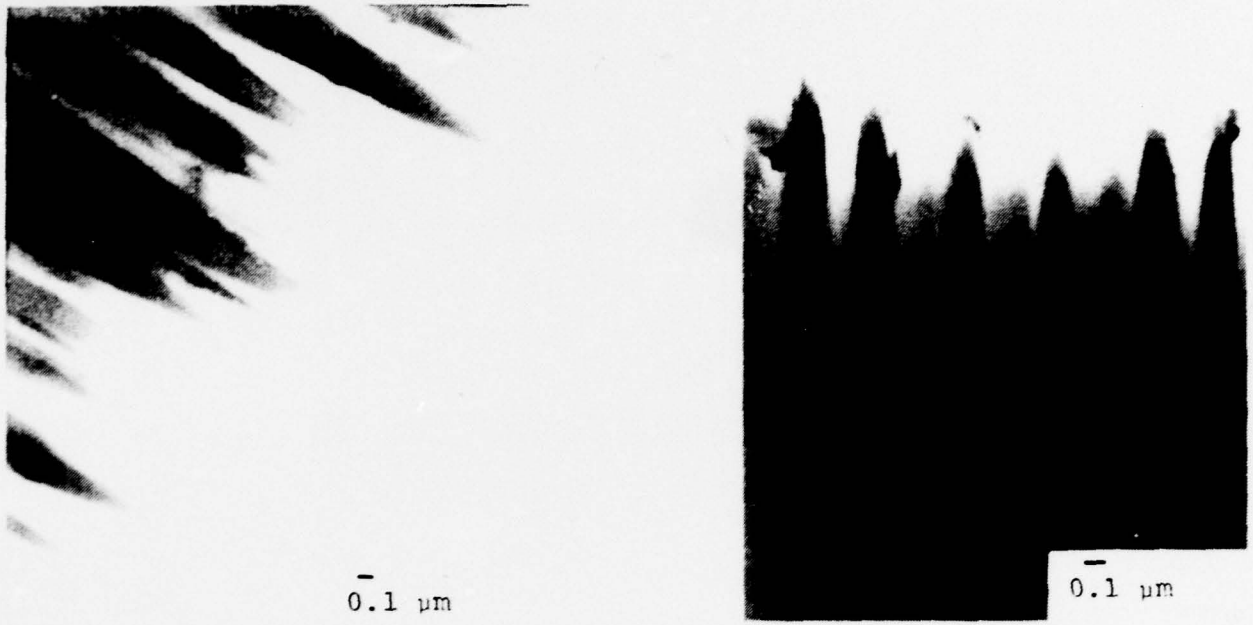

Rod structure in outside region of as-produced boron filament.

Figure 31

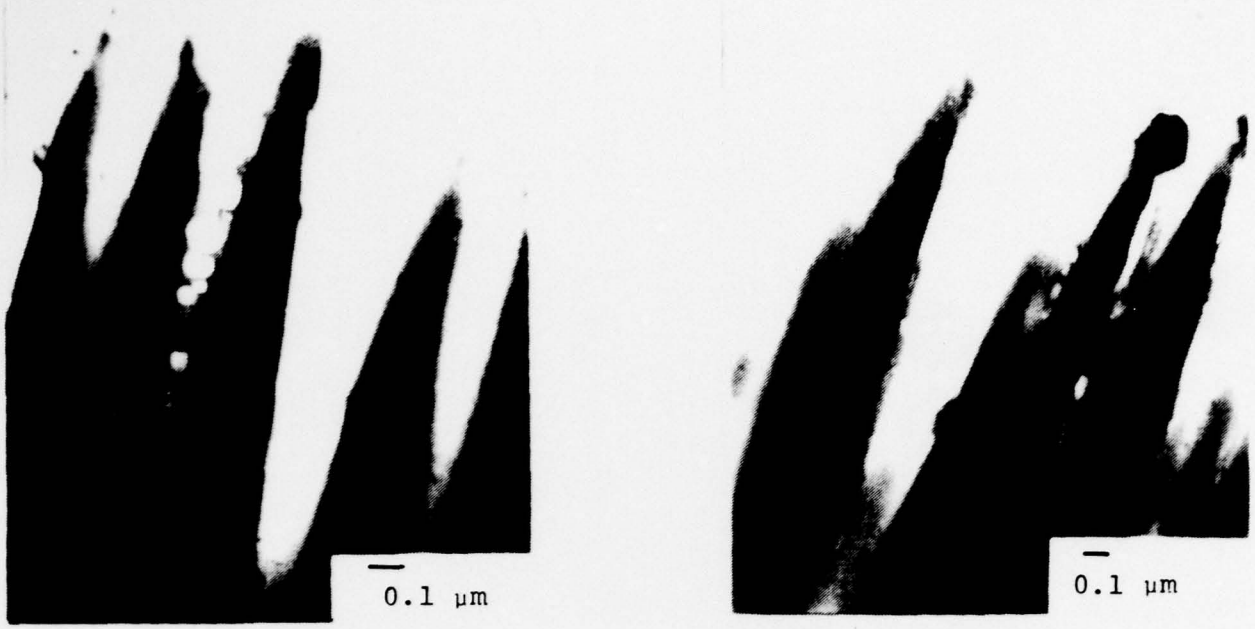

Rod structure in outside region of as-produced boron filament. Typical dimension of void ≈ 500 A.

Figure 32

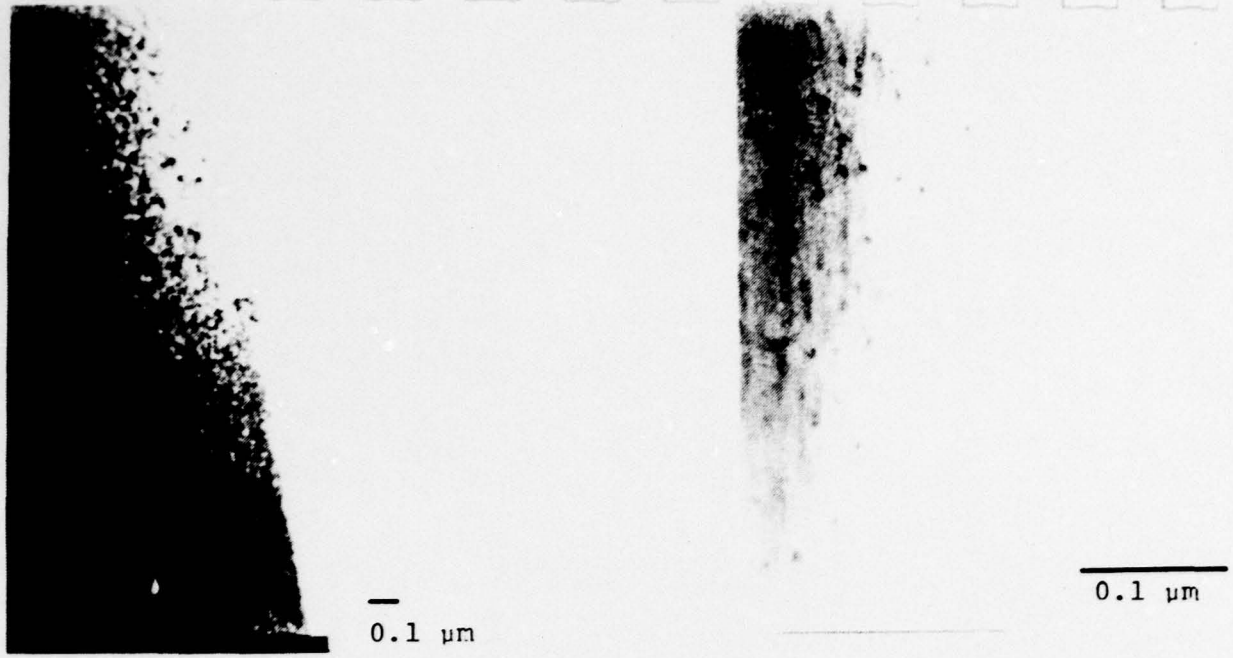

Outside region of as-produced boron filament (rod structure absent). Typical void size ≐ 100 A.

Figure 33

APPENDIX

Development of Transformation Model Let L(r) be the unconstrained length of an infinitesimally thin cylindrical shell of a filament at a distance r from the filament axis, and let $\ell(R)$ be the actual length of a filament with outside radius R. Assume that the radial growth of the filament is linear in time:

$$R = r_c + \alpha t$$

or

$$t = R - r_c/\alpha \qquad (a)$$

where

$r_c \equiv$ the core radius

$\alpha \equiv$ the growth rate $\left(\frac{dR}{dt}\right)$.

Assume that the boron outside the core transforms from its initial deposited length to a structure with an unconstrained length that is f times greater with a rate constant K such that:

$$L(r) = L_0(r)\left[1 + (f - 1)\left(1 - e^{-K(t - t'(r))}\right)\right] \qquad (b)$$

where, $L_0(r) \equiv$ length when deposited, or

$$L_0(r) = \ell(R)\Big|_{R = r} \qquad (c)$$

and $t'(r) \equiv$ the time at which it was deposited, or

$$t'(r) = t(R)\Big|_{R = r} . \qquad (d)$$

Then, by substitution into equation (b) from (a), (c) and (d):

$$L(r) = \ell(r)\left[1 + (f - 1)\,(1 - e^{K/\alpha(R - r)})\right],\ r_c \leq r \leq R \qquad (e)$$

The axial strain and stress in the boron sheath are then:

$$\left.\begin{aligned} \varepsilon(r) &= \frac{\ell(R) - L(r)}{L(r)} \\ \sigma(r) &= E\varepsilon(r) \end{aligned}\right\} \quad r_c \leq r \leq R \qquad (f)$$

where

$E \equiv$ Young's modulus of the boron sheath, (assumed constant).

However, if $\varepsilon(r) \geq \varepsilon_{max}$ or $\leq \varepsilon_{min}$ assume non-elastic deformation takes place such that:

$$\ell(r) = \frac{\ell(R)}{e_{max} + 1}\ \frac{1}{1 + (f - 1)\,(1 - e^{-K/\alpha(R - r)})} \qquad (g)$$

or

$$\ell(r) = \frac{\ell(R)}{e_{min} + 1}\ \frac{1}{1 + (f - 1)\,(1 - e^{-K/\alpha(R - r)})}\ .$$

As boron diffuses into the core, assume that the core transforms from its initial state to a structure with an unconstrained length f_c times greater with a rate constant K_c such that:

$$L(r) = \ell(r_c)\left[1 + S\,(t - t''(r))\,(f_c - 1)(1 - e^{-K_c(t - t''(r))}\right],$$
$$0 \leq r \leq r_c \qquad (h)$$

where

$t''(r) \equiv$ the time at which this transformation starts taking place

$S(t - t''(r)) \equiv$ a step function such that $S(X) = 0$, $X \leq 0$; $S(X) = 1$, $X > 0$

Now assume the diffusion of boron into the core is linear in

time so that the radius at which the transformation is starting to take place is:

$$r = r_c - \beta t'', \quad 0 \leq r \leq r_c \ . \tag{i}$$

Then, from (a):

$$t - t'' = \frac{R - r_c}{\alpha} + \frac{r - r_c}{\beta} \ . \tag{j}$$

Substitution into equation (f) gives:

$$L(r) = \ell(r_c)\left[1+S\left(\frac{R-r_c}{\alpha} - \frac{r_c-r}{\beta}\right)(f_c-1)\left(1-e^{-K_c\left(\frac{R-r_c}{\alpha} - \frac{r_c-r}{\beta}\right)}\right)\right],$$

$$0 \leq r \leq r_c \ . \tag{k}$$

The axial strain and stress in the core are then:

$$\left.\begin{aligned} \varepsilon(r) &= \frac{\ell(R) - L(r)}{L(r)} \\ \sigma(r) &= E_c \varepsilon(r) \end{aligned}\right\} \quad 0 \leq r \leq r_c \tag{l}$$

where

$E_c \equiv$ Young's modulus of the core (assumed constant).

However, if $\varepsilon(r) \geq \varepsilon_{c_{max}}$ or $\leq \varepsilon_{c_{min}}$, assume the transformation is limited such that:

$$L(r) = \frac{\ell(R)}{\varepsilon_{c_{max}} + 1} \tag{m}$$

or

$$L(r) = \frac{\ell(R)}{\varepsilon_{c_{min}} + 1}$$

For equilibrium, the integrated axial stress is zero, so:

$$\int_0^{2\pi} \int_0^R \sigma \, r dr d\theta = 0 \tag{n}$$

or, since σ is independent of θ,

$$\int_0^R \sigma \, rdr = 0.$$

Thus,

$$E_c \int_0^{r_c} \left[\frac{\ell(R)-L(r)}{L(r)}\right] rdr + E\int_{r_c}^{R} \left[\frac{\ell(R)-L(r)}{L(r)}\right] rdr = 0. \qquad (o)$$

By rearranging terms:

$$E_c \ell(R) \int_0^{r_c} \frac{rdr}{L(r)} + E\ell(R) \int_{r_c}^{R} \frac{rdr}{L(r)} = E_c \frac{r_c^2}{2} + E \frac{(R^2-r_c^2)}{2}^{(p)}.$$

Substitution and rearrangement gives:

$$\frac{\ell(R)}{\ell(r_c)} = \frac{\frac{1}{2}\left[R^2 + \left(\frac{E_c}{E} - 1\right) r_c^2\right]}{\frac{E_c}{E}\int_0^{r_c} \frac{rdr}{1+S\left(\frac{R-r_c}{\alpha} - \frac{r_c-r}{\beta}\right)(f_c-1)\left[1-e^{-K_c\left(\frac{R-r_c}{\alpha} - \frac{r_c-r}{\beta}\right)}\right]}} \qquad (q)$$

$$+ \int_{r_c}^{R} \frac{\ell(r_c)\, rdr}{\ell(r)\left[1 + (f-1)\left(1 - e^{-K/\alpha(R-r)}\right)\right]}.$$

This equation respresents the elongation as a function of filament radius.

Let $R_n = r_c + n\Delta r$, and $X_n = \frac{\ell(R_n)}{\ell(r_c)}$,

where

$R_n \equiv$ filament radius after $n^{\underline{th}}$ shell is deposited

$n \equiv$ number of $n^{\underline{th}}$ shell

$\Delta r \equiv$ shell thickness.

Divide the core into m shells. Set $U_i = 1$, $i = 0 \ldots m$ and let:

$$Z_{ni} = 1+S\left(\frac{n\Delta r}{\alpha} - \frac{(1-i/m)\,r_c}{\beta}\right)(f_c-1)\left[1-e^{-K_c\left(\frac{n\Delta r}{\alpha}-\frac{(1-i/m)\,r_c}{\beta}\right)}\right] \tag{r}$$

$$i = 0 \;\; . \; . \; m$$

$$\text{If } U_i \leq \frac{X_n}{Z_{ni}(\varepsilon_{c_{max}} + 1)}, \text{ set } U_i = \frac{X_n}{Z_{ni}(\varepsilon_{c_{max}} + 1)}$$

$$\text{If } U_i \geq \frac{X_n}{Z_{ni}(\varepsilon_{c_{min}} + 1)}, \text{ set } U_i = \frac{X_n}{Z_{ni}(\varepsilon_{c_{min}} + 1)} \tag{s}$$

Then,

$$\int_0^{r_c} \frac{rdr}{\frac{\ell(r)}{\ell(r_c)}\left\{1+S\left(\frac{n\Delta r}{\alpha} - \frac{(1-i/m)\,r_c}{\beta}\right)(f_c-1)\left[1-e^{-K_c\left(\frac{n\Delta r}{\alpha} - \frac{(i-i/m)\,r_c}{\beta}\right)}\right]\right\}}$$

$$= \frac{r_c^2}{m^2} - \sum_{i=0}^{m} \frac{V_i\, i}{U_i Z_{ni}} \tag{t}$$

$$V_i = 1/2;\; i = 0,\; m$$

$$V_i = 1;\; i \neq 0, m$$

Also let,

$$Y_{ni} = 1 + (f - 1)\left[1 - e^{-K/\alpha(n - i)\Delta r}\right] \tag{u}$$

$$\text{If } X_i \leq \frac{X_n}{Y_{ni}(\varepsilon_{max} + 1)}, \text{ set } X_i = \frac{X_n}{Y_{ni}(\varepsilon_{max} + 1)}$$

$$\text{If } X_i \geq \frac{X_n}{Y_{ni}(\varepsilon_{min} + 1)}, \text{ set } X_i = \frac{X_n}{Y_{ni}(\varepsilon_{min} + 1)} \tag{v}$$

Therefore, with

$$W_i = 1/2;\; i = 0$$

$$W_i = 1;\; i \neq 0,$$

$$\int_{r_c}^{R} \frac{rdr}{\frac{\ell(r)}{\ell(r_c)}\left[1 + (f - 1)\ (1 - e^{-K/\alpha(A - i)\Delta r})\right]} = \tag{w}$$

$$\Delta r \sum_{i=0}^{n-1} \frac{W_i\ (r_c + i\Delta r)}{X_i\ Y_{ni}} + \frac{\Delta r}{2} \frac{r_c + n\Delta r}{X_n} ,$$

by substitution and rearrangement of terms yields,

$$X_n = \frac{\frac{1}{2}\left[\frac{E_c}{E}\ r_c^{\,2} + 2r_c n\Delta r + n^2\Delta r^2\right]}{\frac{E_c}{E}\frac{r_c^{\,2}}{m}\sum_{i=0}^{m}\frac{V_i\ i}{U_i\ Z_{ni}} + \Delta r\sum_{i=0}^{n-1}\frac{W_i\ (r_c + i\Delta r)}{X_i\ Y_{ni}} + \frac{\Delta r}{2}\frac{r_c + n\Delta r}{X_n}} \tag{x}$$

or

$$X_n = \frac{\frac{1}{2}\left[\frac{E_c}{E}\ r_c^{\,2} + 2r_c n\Delta r + n^2\Delta r^2 - r_c\Delta r - n\Delta r^2\right]}{\frac{E_c}{E}\frac{r_c^{\,2}}{m}\sum_{i=0}^{m}\frac{V_i\ i}{U_i\ Z_{ni}} + \Delta r\sum_{i=0}^{n-1}\frac{W_i(r_c + i\Delta r)}{X_i\ Y_{ni}}} \tag{y}$$

and $X_n = 1 + A/100$

where

A ≡ elongation expressed in %.

SECURITY CLASSIFICATION OF THIS PAGE (When Data Entered)

REPORT DOCUMENTATION PAGE		READ INSTRUCTIONS BEFORE COMPLETING FORM
1. REPORT NUMBER No. 2	2. GOVT ACCESSION NO.	3. RECIPIENT'S CATALOG NUMBER
4. TITLE (and Subtitle) Investigation of Elongation and Its Relationship to Residual Stresses in Boron Filaments		5. TYPE OF REPORT & PERIOD COVERED 6. PERFORMING ORG. REPORT NUMBER
7. AUTHOR(s) F. E. Wawner, Jr.		8. CONTRACT OR GRANT NUMBER(s) N00014-76-C-0694
9. PERFORMING ORGANIZATION NAME AND ADDRESS Department of Materials Science, SEAS University of Virginia, Thornton Hall Charlottesville, Virginia 22901		10. PROGRAM ELEMENT, PROJECT, TASK AREA & WORK UNIT NUMBERS
11. CONTROLLING OFFICE NAME AND ADDRESS Department of the Navy Office of Naval Research Arlington, Virginia 22217		12. REPORT DATE September 1979 13. NUMBER OF PAGES
14. MONITORING AGENCY NAME & ADDRESS (if different from Controlling Office)		15. SECURITY CLASS. (of this report) Unclassified 15a. DECLASSIFICATION/DOWNGRADING SCHEDULE

16. DISTRIBUTION STATEMENT (of this Report)

Distribution of this document is unlimited.

17. DISTRIBUTION STATEMENT (of the abstract entered in Block 20, if different from Report)

18. SUPPLEMENTARY NOTES

19. KEY WORDS (Continue on reverse side if necessary and identify by block number)

20. ABSTRACT (Continue on reverse side if necessary and identify by block number)

Elongation in boron filament during fabrication was investigated and found to be as great as 16% under certain conditions. It was also found to obey a relatively simple empirical relationship which yielded effective activation energies. A model for the elongation was proposed, and a computer program was designed to simulate the deposition and elongation of boron on a tungsten wire substrate. Internal residual stress distribution

DD FORM 1 JAN 73 1473 EDITION OF 1 NOV 65 IS OBSOLETE

SECURITY CLASSIFICATION OF THIS PAGE (When Data Entered)

AD-A074 440 VIRGINIA UNIV CHARLOTTESVILLE DEPT OF MATERIALS SCIENCE F/G 11/6
INVESTIGATION OF ELONGATION AND ITS RELATIONSHIP TO RESIDUAL ST--ETC(U)
SEP 79 F E WAWNER, J W EASON, R A JOHNSON N00014-76-C-0694

UNCLASSIFIED UVA/525322/MS79/102 NL

2 OF 2
AD A074440

END
DATE FILMED
10-79
DDC

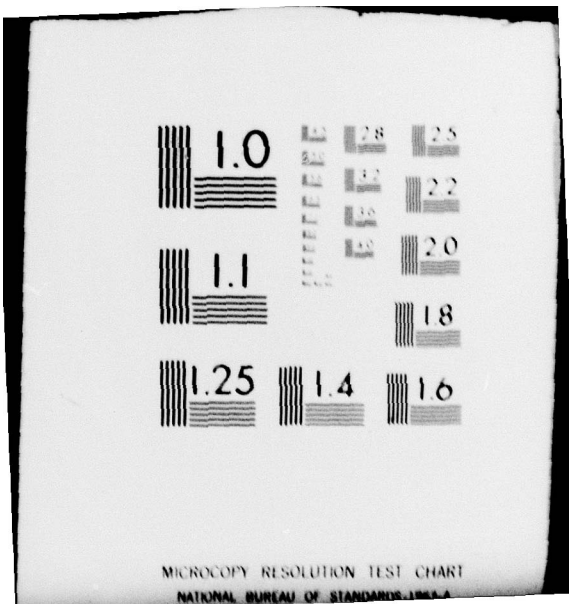
1.0
1.1
1.25
1.4
1.6
2.8
2.5
2.2
2.0
1.8
MICROCOPY RESOLUTION TEST CHART
NATIONAL BUREAU OF STANDARDS-1963-A

of boron/tungsten filament were also generated by the computer program. Good agreement was found between the proposed model and experimental results. Negative elongation (contraction) of boron filament was observed during annealing and found to be dependent upon the concentration of oxygen present in the annealing atmosphere. The contraction was also found to be the result of void formation at the core-boron sheath interface. The contraction obeyed an empirical relationship, which represented an exponential decay toward equilibrium from a non-equilibrium state and an effective activation energy was determined for boron/tungsten filament.

DISTRIBUTION LIST

Copy No.	
1	Office of Naval Research 800 N. Quincy Street Arlington, VA 22217
2 - 56	See Basic Distribution List
57 - 93	See Supplementary Distribution List
94	Office of Naval Research Resident Representative 2110 G Street, N. W. Washington, D. C. 20037 Attn: C. R. Main Administrative Contracting Officer
95 - 115	F. E. Wawner, Jr.
116	K. R. Lawless
117	I. A. Fischer Office of Sponsored Programs
118 - 119	E. H. Pancake Clark Hall
120	RLES Files

JO# 0258 JDH

BASIC DISTRIBUTION LIST

Technical and Summary Reports April 1978

Organization	Copies
Defense Documentation Center Cameron Station Alexandria, VA 22314	12
Office of Naval Research Department of the Navy 800 N. Quincy Street Arlington, VA 22217	
ATTN: Code 471	1
Code 102	1
Code 470	1
Commanding Officer Office of Naval Research Branch Office Building 114, Section D 666 Summer Street Boston, MA 02210	1
Commanding Officer Office of Naval Research Branch Office 536 South Clark Street Chicago, IL 60605	1
Office of Naval Research San Francisco Area Office 760 Market Street, Room 447 San Francisco, CA 94102	1
Naval Research Laboratory Washington, DC 20375	
ATTN: Codes 6000	1
6100	1
6300	1
6400	1
2627	1
Naval Air Development Center Code 302 Warminster, PA 18964 ATTN: Mr. F. S. Williams	1

Organization	Copies
Naval Air Propulsion Test Center Trenton, NJ 08628 ATTN: Library	1
Naval Construction Batallion Civil Engineering Laboratory Port Hueneme, CA 93043 ATTN: Materials Division	1
Naval Electronics Laboratory San Diego, CA 92152 ATTN: Electron Materials Sciences Division	1
Naval Missile Center Materials Consultant Code 3312-1 Point Mugu, CA 92041	1
Commanding Officer Naval Surface Weapons Center White Oak Laboratory Silver Spring, MD 20910 ATTN: Library	1
David W. Taylor Naval Ship Research and Development Center Materials Department Annapolis, MD 21402	1
Naval Undersea Center San Diego, CA 92132 ATTN: Library	1
Naval Underwater System Center Newport, RI 02840 ATTN: Library	1
Naval Weapons Center China Lake, CA 93555 ATTN: Library	1
Naval Postgraduate School Monterey, CA 93940 ATTN: Mechanical Engineering Department	1

BASIC DISTRIBUTION LIST (cont'd)

Organization	Copies
Naval Air Systems Command Washington, DC 20360 ATTN: Codes 52031 52032	1
Naval Sea System Command Washington, DC 20362 ATTN: Code 035	1
Naval Facilities Engineering Command Alexandria, VA 22331 ATTN: Code 03	1
Scientific Advisor Commandant of the Marine Corps Washington, DC 20380 ATTN: Code AX	1
Naval Ship Engineering Center Department of the Navy Washington, DC 20360 ATTN: Code 6101	1
Army Research Office P.O. Box 12211 Triangle Park, NC 27709 ATTN: Metallurgy & Ceramics Program	1
Army Materials and Mechanics Research Center Watertown, MA 02172 ATTN: Research Programs Office	1
Air Force Office of Scientific Research Bldg. 410 Bolling Air Force Base Washington, DC 20332 ATTN: Chemical Science Directorate Electronics & Solid State Sciences Directorate	1 1
Air Force Materials Laboratory Wright-Patterson AFB Dayton, OH 45433	1
Library Building 50, Rm 134 Lawrence Radiation Laboratory Berkeley, CA	1

Organization	Copies
NASA Headquarters Washington, DC 20546 ATTN: Code RRM	1
NASA Lewis Research Center 21000 Brookpark Road Cleveland, OH 44135 ATTN: Library	1
National Bureau of Standards Washington, DC 20234 ATTN: Metallurgy Division Inorganic Materials Div.	1 1
Director Applied Physics Laboratory University of Washington 1013 Northeast Forthieth Street Seattle, WA 98105	1
Defense Metals and Ceramics Information Center Battelle Memorial Institute 505 King Avenue Columbus, OH 43201	1
Metals and Ceramics Division Oak Ridge National Laboratory P.O. Box X Oak Ridge, TN 37380	1
Los Alamos Scientific Laboratory P.O. Box 1663 Los Alamos, NM 87544 ATTN: Report Librarian	1
Argonne National Laboratory Metallurgy Division P.O. Box 229 Lemont, IL 60439	1
Brookhaven National Laboratory Technical Information Division Upton, Long Island New York 11973 ATTN: Research Library	1
Office of Naval Research Branch Office 1030 East Green Street Pasadena, CA 91106	1

M
January 1978

SUPPLEMENTARY DISTRIBUTION LIST

Technical and Summary Reports

Professor G. S. Ansell
Rensselaer Polytechnic Institute
Dept. of Metallurgical Engineering
Troy, New York 12181

Professor H. K. Birnbaum
University of Illinois
Department of Metallurgy
Urbana, Illinois 61801

Dr. E. M. Breinan
United Aircraft Corporation
United Aircraft Res. Laboratories
East Hartford, Connecticut 06108

Professor H. D. Brody
University of Pittsburgh
School of Engineering
Pittsburgh, Pennsylvania 14213

Mr. P. J. Cacciatore
General Dynamics
Electric Boat Division
Eastern Point Road
Groton, Connecticut 06340

Professor J. B. Cohen
Northwestern University
Dept. of Material Sciences
Evanston, Illinois 60201

Professor M. Cohen
Massachusetts Institute of Technology
Department of Metallurgy
Cambridge, Massachusetts 02139

Professor Thomas W. Eagar
Massachusetts Institute of Technology
Department of Materials
Science and Engineering
Cambridge, Massachusetts 02139

Professor B. C. Giessen
Northeastern University
Department of Chemistry
Boston, Massachusetts 02115

Dr. G. T. Hahn
Battelle Memorial Institute
Department of Metallurgy
505 King Avenue
Columbus, Ohio 43201

Professor D. G. Howden
Ohio State University
Dept. of Welding Engineering
190 West 19th Avenue
Columbus, Ohio 43210

Dr. C. S. Kortovich
TRW, Inc.
23555 Euclid Avenue
Cleveland, Ohio 44117

Professor D. A. Koss
Michigan Technological University
College of Engineering
Houghton, Michigan 49931

Professor A. Lawley
Drexel University
Dept. of Metallurgical Engineering
Philadelphia, Pennsylvania 19104

Professor Harris Marcus
The University of Texas at Austin
College of Engineering
Austin, Texas 78712

Dr. H. Margolin
Polytechnic Institute of New York
333 Jay Street
Brooklyn, New York 11201

Professor K. Masubuchi
Massachusetts Institute of Technology
Department of Ocean Engineering
Cambridge, Massachusetts 02139

Dr. H. I. McHenry
National Bureau of Standards
Institute for Basic Standards
Boulder, Colorado 80302

SUPPLEMENTARY DISTRIBUTION LIST (Cont'd)

Professor J. W. Morris, Jr.
University of California
College of Engineering
Berkeley, California 94720

Professor Ono
University of California
Materials Department
Los Angeles, California 90024

Dr. Neil E. Paton
Rockwell International
Science Center
1049 Camino Dos Rios
P.O. Box 1085
Thousand Oaks, California 91360

Mr. A. Pollack
Naval Ships Research & Development
Center
Annapolis, Maryland 21402

Dr. Karl M. Prewo
United Technologies Laboratories
United Technologies Corporation
East Hartford, Connecticut 06108

Professor W. F. Savage
Rensselaer Polytechnic Institute
School of Engineering
Troy, New York 12181

Professor O. D. Sherby
Stanford University
Materials Sciences Division
Stanford, California 94300

Professor J. Shyne
Stanford University
Materials Sciences Division
Stanford, California 94300

Dr. R. P. Simpson
Westinghouse Electric Corporation
Research & Development Center
Pittsburgh, Pennsylvania 15235

Dr. E. A. Starke, Jr.
Georgia Institute of Technology
School of Chemical Engineering
Atlanta, Georgia 30332

Professor David Turnbull
Harvard University
Division of Engineering and
Applied Physics
Cambridge, Massachusetts 02139

Dr. F. E. Wawner
University of Virginia
School of Engineering and Applied
Science
Charlottesville, Virginia 22901

Dr. C. R. Whitsett
McDonnell Douglas Research
McDonnell Douglas Corporation
Saint Louis, Missouri 63166

Dr. J. C. Williams
Carnegie-Mellon University
Department of Metallurgy and
Materials Sciences
Schenley Park
Pittsburgh, Pennsylvania 15213

Professor H. G. F. Wilsdorf
University of Virginia
Charlottesville, Virginia 22903

Dr. M. A. Wright
University of Tennessee
Space Institute
Tullahoma, Tennessee 37388

Dr. J. A. DiCarlo
Lewis Research Center
NASA
Mail Stop 106-1
Cleveland, Ohio 44135

T. J. Reinhart, Jr., Chief
Composite & Fibrous Materials Branch
AFML
Department of Air Force
Wright-Patterson AFB, Ohio 45433

Mr. G. B. Barthold
Aluminum Company of America
1200 Ring Bldg.
Washington, D. C. 20036

UNIVERSITY OF VIRGINIA

School of Engineering and Applied Science

The University of Virginia's School of Engineering and Applied Science has an undergraduate enrollment of approximately 1,300 students with a graduate enrollment of approximately 500. There are 125 faculty members, a majority of whom conduct research in addition to teaching.

Research is an integral part of the educational program and interests parallel academic specialties. These range from the classical engineering departments of Chemical, Civil, Electrical, and Mechanical and Aerospace to departments of Biomedical Engineering, Engineering Science and Systems, Materials Science, Nuclear Engineering and Engineering Physics, and Applied Mathematics and Computer Science. In addition to these departments, there are interdepartmental groups in the areas of Automatic Controls and Applied Mechanics. All departments offer the doctorate; the Biomedical and Materials Science Departments grant only graduate degrees.

The School of Engineering and Applied Science is an integral part of the University (approximately 1,530 full-time faculty with a total enrollment of about 16,000 full-time students), which also has professional schools of Architecture, Law, Medicine, Commerce, and Business Administration. In addition, the College of Arts and Sciences houses departments of Mathematics, Physics, Chemistry and others relevant to the engineering research program. This University community provides opportunities for interdisciplinary work in pursuit of the basic goals of education, research, and public service.